Molecular Cell

Article

BRCA1 levels and DNA-damage response are controlled by the competitive binding of *circHIPK3* or FMRP to the *BRCA1* mRNA

Graphical abstract

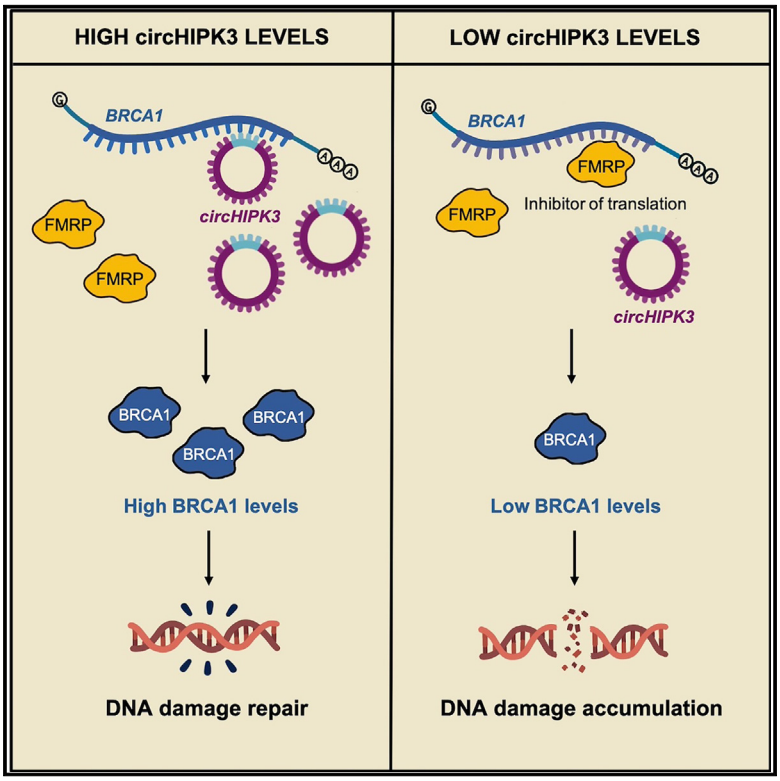

Highlights

- circHIPK3 and FMRP compete for a direct site-specific binding to the *BRCA1* mRNA
- circHIPK3 promotes BRCA1 expression, preventing FMRP-mediated translational inhibition
- circHIPK3-*BRCA1* interaction disruption sensitizes cancer cells to DNA-damaging drugs
- FMRP-*BRCA1*-binding disruption restores normal BRCA1 levels in BRCA1 hemizygous cells

Authors

Chiara Grelloni, Raffaele Garraffo, Adriano Setti, ..., Marco Alessandro Pierotti, Manuel Beltran, Irene Bozzoni

Correspondence

manuel.beltrannebot@uniroma1.it (M.B.), irene.bozzoni@uniroma1.it (I.B.)

In brief

Grelloni et al. demonstrate that the tumor-associated circular RNA circHIPK3 and the RNA-binding protein FMRP compete for site-specific binding to the *BRCA1* mRNA. CircHIPK3, by interacting with the *BRCA1* transcript, prevents FMRP-mediated translational inhibition, thereby increasing BRCA1 protein levels. These interactions represent novel therapeutic targets to modulate BRCA1 levels.

Grelloni et al., 2024, Molecular Cell *84*, 1–16
November 7, 2024
https://doi.org/10.1016/j.molcel.2024.09.016

CellPress

Molecular Cell

CellPress
OPEN ACCESS

Article

BRCA1 levels and DNA-damage response are controlled by the competitive binding of *circHIPK3* or FMRP to the *BRCA1* mRNA

Chiara Grelloni,[1] Raffaele Garraffo,[1] Adriano Setti,[1] Francesca Rossi,[1,5] Giovanna Peruzzi,[2] Mario Cinquanta,[3] Maria Carmela Di Rosa,[4] Marco Alessandro Pierotti,[3] Manuel Beltran,[1,*] and Irene Bozzoni[1,2,6,*]

[1]Department of Biology and Biotechnology Charles Darwin, Sapienza University of Rome, 00185 Rome, Italy
[2]Center for Life Nano- & Neuro-Science, Fondazione Istituto Italiano di Tecnologia (IIT), 00161 Rome, Italy
[3]Cogentech ltd Benefit C. Registered Office, 20133 Milan, Italy
[4]Local Unit c/o Scientific & Technologic Park of Sicily, 95121 Catania, Italy
[5]Present address: Immunology Programme, The Babraham Institute, Babraham Research Campus, Cambridge CB22 3AT, UK
[6]Lead contact
*Correspondence: manuel.beltrannebot@uniroma1.it (M.B.), irene.bozzoni@uniroma1.it (I.B.)
https://doi.org/10.1016/j.molcel.2024.09.016

SUMMARY

Circular RNAs (circRNAs) are covalently closed RNA molecules widely expressed in eukaryotes and deregulated in several pathologies, including cancer. Many studies point to their activity as microRNAs (miRNAs) and protein sponges; however, we propose a function based on circRNA-mRNA interaction to regulate mRNA fate. We show that the widely tumor-associated *circHIPK3* directly interacts *in vivo* with the *BRCA1* mRNA through the back-splicing region in human cancer cells. This interaction increases *BRCA1* translation by competing for the binding of the fragile-X mental retardation 1 protein (FMRP) protein, which we identified as a *BRCA1* translational repressor. *CircHIPK3* depletion or disruption of the circRNA-mRNA interaction decreases BRCA1 protein levels and increases DNA damage, sensitizing several cancer cells to DNA-damage-inducing agents and rendering them susceptible to synthetic lethality. Additionally, blocking FMRP interaction with *BRCA1* mRNA with locked nucleic acid (LNA) restores physiological protein levels in BRCA1 hemizygous breast cancer cells, underscoring the importance of this circRNA-mRNA interaction in regulating DNA-damage response.

INTRODUCTION

Intermolecular RNA-RNA interactions are at the basis of many regulatory processes of gene expression control. As far as mRNA fate is concerned, most of the studies have focused on the role played by microRNAs (miRNAs) or long non-coding RNAs (lncRNAs) in controlling mRNA localization, stability, and translation.[1,2] More recently, growing interest has been dedicated to the study of circular RNAs (circRNAs), covalently closed circular molecules originating from an alternative splicing event known as back-splicing. This family of non-coding RNAs (ncRNAs) is thrilling not only because of their evolutionary conservation and tissue-specific expression but also, mainly, for their altered expression in various pathological conditions, particularly cancer.[3,4] In this work, we studied *circHIPK3*, officially named *circHIPK3(2)* (circBase: hsa_circ_0000284), a circRNA widely upregulated in a diverse set of cancers.[5–9] This wide-range *circHIPK3* upregulation of *circHIPK3* commonly correlates with more aggressive oncogenic phenotypes, involving increased proliferation and migration. However, despite the evident association between *circHIPK3* upregulation and oncogenic development, a unified molecular mechanism underlying its function in different cancers has not been described yet.

Here, we describe the means by which, in rhabdomyosarcoma cell lines, *circHIPK3* directly pairs with several mRNAs *in vivo* and, particularly, with the *BRCA1* mRNA, which, as a result of this interaction, is stabilized and more efficiently translated. The dissection of the underlying molecular mechanism indicated that *circHIPK3-BRCA1* mRNA pairing competes for the binding of the fragile-X mental retardation 1 protein (FMRP) protein on the *BRCA1* transcript. We show that FMRP, known to control mRNA stability and translation,[10–14] is a negative regulator of *BRCA1* translation and that its repressive effect inversely correlates with *circHIPK3* presence.

We also indicate that blocking the interaction between *circHIPK3* and *BRCA1* mRNA decreases BRCA1 protein levels and directly impacts DNA-damage response (DDR) and sensitivity to different DNA-damage-inducing drugs. Moreover, we also show that locked nucleic acids (LNAs) blocking the interaction between FMRP and *BRCA1* restore physiological protein levels

Please cite this article in press as: Grelloni et al., BRCA1 levels and DNA-damage response are controlled by the competitive binding of *circHIPK3* or FMRP to the *BRCA1* mRNA, Molecular Cell (2024), https://doi.org/10.1016/j.molcel.2024.09.016

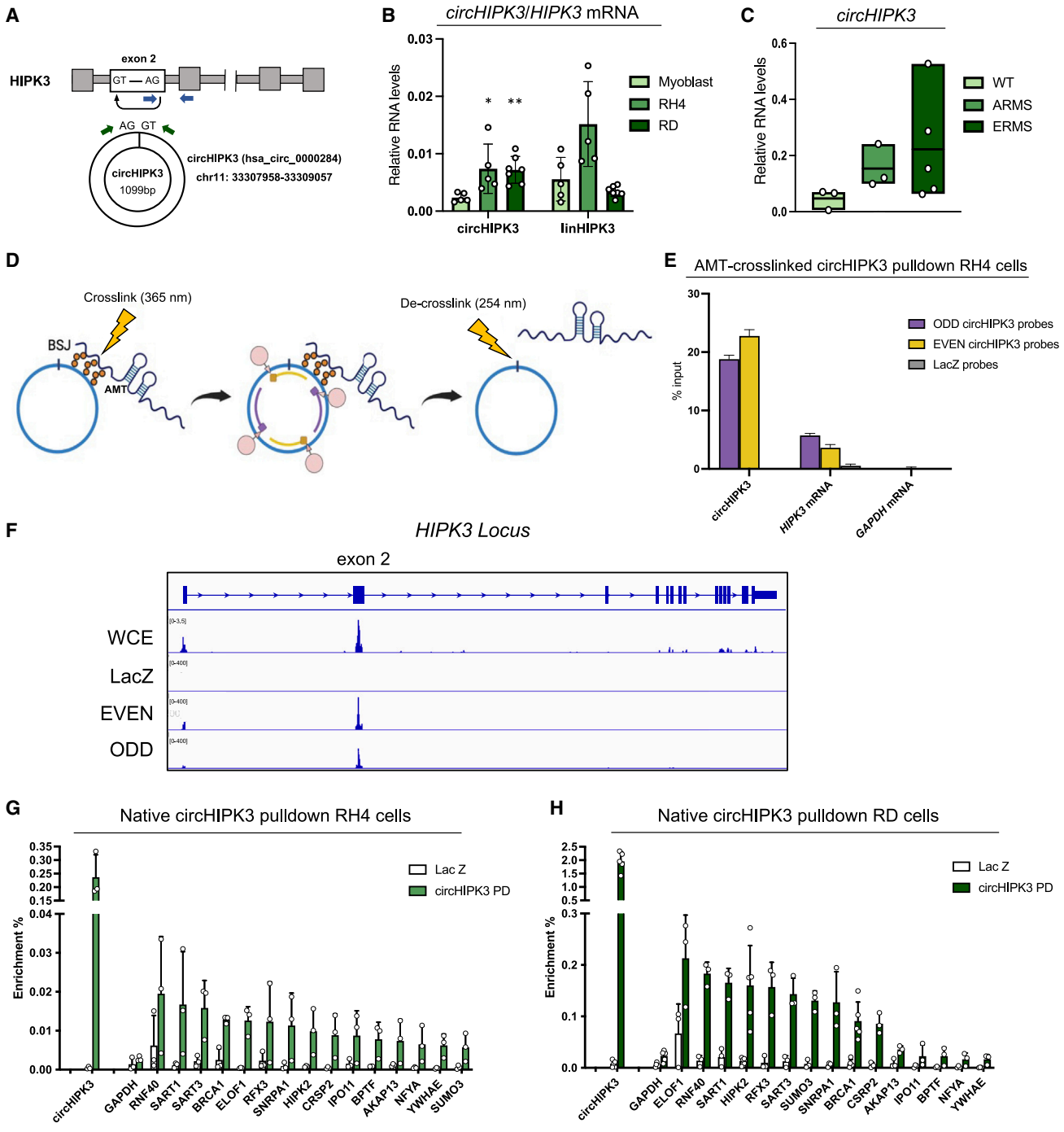

Figure 1. *CircHIPK3* is upregulated in rhabdomyosarcoma cells and interacts with several mRNAs *in vivo*

(A) Schematic representation of *circHIPK3* formation through HIPK3 exon-2 back-splicing. Green and blue arrows represent the oligonucleotides used to amplify *circHIPK3* and *HIPK3*, respectively.

(B) RNA levels (rel. to *GAPDH*) of *circHIPK3* and *HIPK3* mRNA in wild-type (WT) human primary myoblasts, RH4 cell line (ARMS) (circHIPK3, $p = 0.033$), and RD cell line (ERMS) (circHIPK3, $p = 0.0014$). $n > 3$. Data are represented as mean ± SD.

(C) RNA levels (rel. to *GAPDH*) of *circHIPK3* in healthy skeletal muscle (WT, $n = 3$), alveolar RMS (ARMS, $n = 3$), and embryonal RMS (ERMS, $n = 5$) samples from pediatric age-matched patients.

(D) Cartoon representing *circHIPK3* pull-down approach with AMT (4′aminomethyl- 4,5′-8 trimethylpsoralen). ODD and EVEN biotinylated probes are represented in violet and yellow, respectively, while streptavidin beads are represented in pink.

(legend continued on next page)

in BRCA1 hemizygous breast cancer cells, setting the regulation of this interaction as an attractive therapeutic strategy to improve tumor treatment.

RESULTS

CircHIPK3 is upregulated in rhabdomyosarcoma cells and interacts with several mRNAs *in vivo*

Previous data indicated that *circHIPK3* is one of the most upregulated circRNA species in rabdomyosarcoma.[15] This finding, together with its increased levels in a large variety of different tumors, prioritized its selection for further functional studies. *CircHIPK3* is a covalently closed, 1,099-nucleotide-long RNA molecule generated from back-splicing of the second exon of the HIPK3 gene (Figure 1A).[16] *CircHIPK3* levels are increased in both embryonal (RD) and alveolar (RH4) rhabdomyosarcoma cell lines compared with myoblasts (Figure 1B); interestingly, the *HIPK3* linear mRNA counterpart is increased in RH4 cells but not in RD cells. Moreover, analysis of the expression levels of *circHIPK3* in tumor and healthy donor samples showed increased levels of *circHIPK3* in both embryonal and alveolar subtypes compared with healthy muscle tissue (Figure 1C). *CircHIPK3* has cytoplasmatic localization (Figure S1A) and is indeed a *bona fide* circRNA because it is resistant to RNase R exonuclease digestion (Figure S1B) and its amplicon contains the back-splicing junction (BSJ) (Figure S1C). Moreover, polysome fractionation indicated that, even if it is not a translated species, it is associated to the 40S and 60S fractions, suggesting its possible involvement in the early steps of translation (Figure S1D).

To dig into the molecular mechanism, we performed pull-down experiments of the endogenous *circHIPK3* in rhabdomyosarcoma RH4 cells after treatment with 4′aminomethyl 4,5′-8 trimethylpsoralen (AMT) to crosslink RNA-RNA interactions. Two different sets of 20-nt-long biotinylated probes (randomly named ODD and EVEN) targeting exon 2 of HIPK3, including the back-splicing junction, were used to pull down the circRNA (Figure 1D). A set of probes, designed against the *E. coli* LacZ sequence, was used as a negative control. The circular isoform was specifically enriched with much higher efficiency than the linear isoform or other non-specific RNAs such as *GAPDH* mRNA (Figure 1E). RNA eluates were subjected to high-throughput RNA sequencing (RNA-seq) for target identification, reads were aligned to the reference genome, and genes were considered prevalently enriched when both ODD and EVEN coverages were at least 4-fold greater than input and LacZ coverages. Most reads in the circHIPK3 locus fell in the second exon and not in other parts of the transcript, indicating the prevalent enrichment of the circular isoform and not of the linear counterpart (Figure 1F). Among the enriched species, several mRNAs were detected (Table S1; Figure S1E). Native RNA pull-down was then used to validate these interactors in both RH4 and RD cells. Reverse-transcription quantitative PCR (RT-qPCR) confirmed the specific enrichment of 10–15 mRNAs identified in the AMT pull-down (Figures 1G and 1H).

CircHIPK3 regulates BRCA1 levels through direct circRNA-mRNA interaction

We then conceived an RNAi approach that could specifically downregulate *circHIPK3* and not its linear counterpart. We designed two types of small interfering RNAs (siRNAs) (Figure 2A): the first targeting the circRNA BSJ region (si-circHIPK3), which should confer specificity only for the circular isoform; the second against an exon of the *HIPK3 mRNA* (si-linHIPK3), which should deplete only the linear counterpart. Figure 2B shows the specificity of the designed siRNAs. When we analyzed the levels of the mRNA interactors upon RNAi treatments, we observed that several of them were downregulated specifically upon the depletion of the circular isoform and not of the linear counterpart (Figures 2C and S2A). We selected a few of them and checked whether the protein levels were also specifically affected by *circHIPK3* depletion. Although for two of them, HIPK2 and YWHAE, there was no significant variation (Figure S2B), we observed a reproducible decrease for BRCA1 (Figure 2C). Notably, upon *circHIPK3* knockdown (KD), we did not observe changes in the levels of the nascent BRCA1 pre-mRNA, excluding BRCA1 transcriptional downregulation (Figure S2C). Moreover, transcription-blocking experiments with alpha-amanitin showed a decreased stability of *BRCA1* mRNA, but not of control *GAPDH* (Figure S2D), indicating that the observed phenotype involves post-transcriptional control, likely including stability and translation. To strengthen the specificity of this downregulation, we transfected RD cells with a different siRNA against the *circHIPK3* BSJ (si-circHIPK3-II); we also confirmed with the second siRNA that the depletion of *circHIPK3* was associated with a downregulation of BRCA1 at mRNA and protein levels (Figure S2E).

Because the probes designed for the RNA pull-down do not allow discrimination between the circular and linear isoforms of HIPK3, we checked the specificity of the interaction between *circHIPK3* and *BRCA1* mRNA by performing a *circHIPK3* pull-down in cells treated with si-scr (scrambled) or si-circHIPK3. Figure 2D shows that depletion of *circHIPK3* abrogates *BRCA1* mRNA enrichment. Along this line, we also performed a specific pull-down of the linear *HIPK3* mRNA, and we did not detect any *BRCA1* mRNA association (Figure 2E). All these data confirm that only *circHIPK3* and not its linear counterpart, *HIPK3* mRNA, interacts with the *BRCA1* mRNA

It has been broadly reported that *circHIPK3* can act as a miRNA sponge to regulate genes.[6] Luciferase transfected constructs with the exon 2 of HIPK3 gene or the 3′ UTR of *BRCA1* downstream of the reporter did not show any alteration in the

(E) Enrichment of *circHIPK3*, *HIPK3* mRNA, and *GAPDH* mRNA in one replicate of AMT-crosslinked circHIPK3 and control LacZ pull-downs performed in RH4 cells. Data are shown as mean of enrichment versus input ± SE of technical triplicates.
(F) Normalized Integrative Genomics Viewer (IGV) RNA sequencing reads densities in HIPK3 locus for WCE, ODD, EVEN, and LacZ pull-down.
(G and H) Enrichment of *circHIPK3*, *GAPDH* mRNA (negative control), and some *circHIPK3* candidate interactors in *circHIPK3* native pull-down and control LacZ pull-down performed in RH4 and RD cells. $n = 3$. Data are shown as mean of enrichment versus input ± SD.
See also Figure S1.

Please cite this article in press as: Grelloni et al., BRCA1 levels and DNA-damage response are controlled by the competitive binding of *circHIPK3* or FMRP to the *BRCA1* mRNA, Molecular Cell (2024), https://doi.org/10.1016/j.molcel.2024.09.016

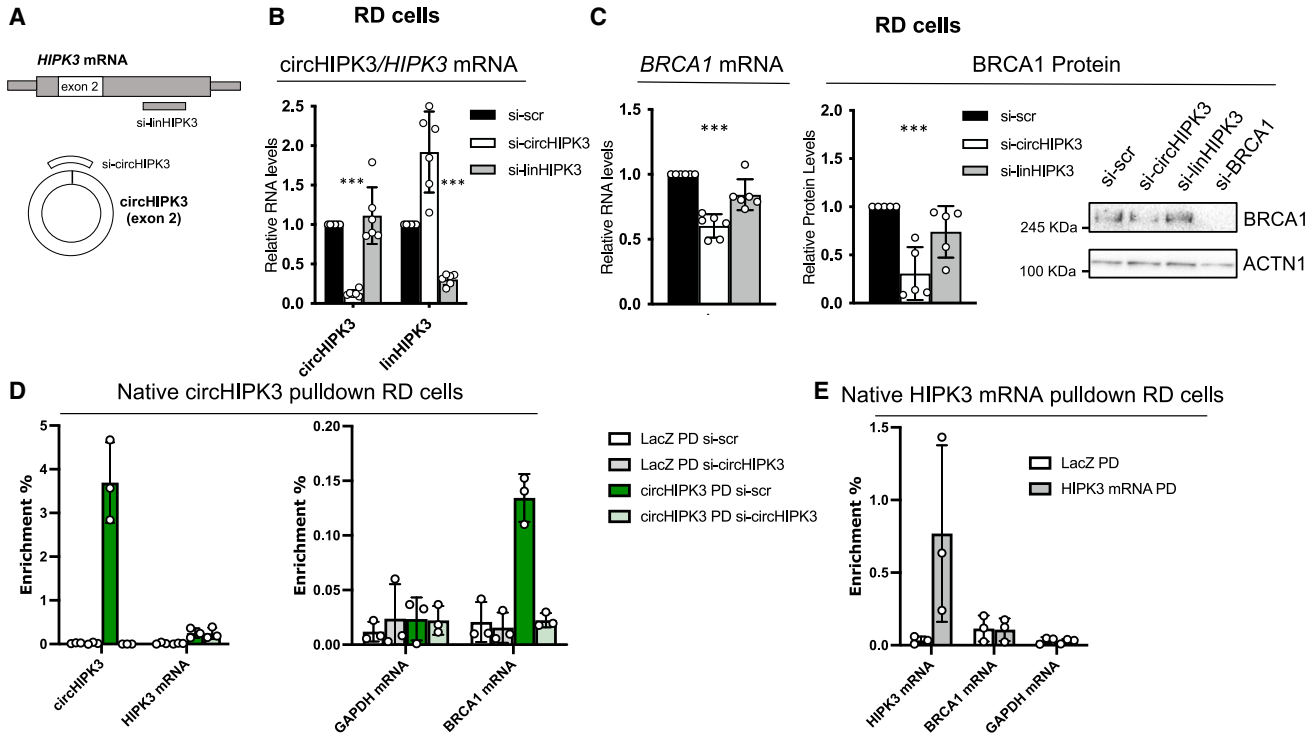

Figure 2. *CircHIPK3* regulates BRCA1 levels through direct RNA-mRNA interaction

(A) Schematic representation of siRNAs targeting *circHIPK3* (si-circHIPK3) and *HIPK3* mRNA (si-linHIPK3).

(B) RNA levels (rel. to *GAPDH*) of *circHIPK3* and *HIPK3* in RD cells in si-scr, si-circHIPK3 (*circHIPK3*, $p < 0.0001$), and si-linHIPK3 (*HIPK3*, $p \leq 0.0001$) conditions. $n > 3$.

(C) Left, RNA levels (rel. to *GAPDH*) of *BRCA1* mRNA in RD cells in si-scr and si-circHIPK3 ($p < 0.0001$). $n > 3$. Right, protein quantification (rel. to loading control) and representative western blot of BRCA1 in RD cells in si-scr, si-circHIPK3 ($p = 0.0005$), and si-linHIPK3 conditions. $n > 3$.

(D) RT-qPCR showing the enrichment of *circHIPK3*, *HIPK3*, *GAPDH* (negative control), and *BRCA1* in *circHIPK3* native pull-down and control LacZ pull-down performed in RD cells in si-scr or si-circHIPK3 conditions. $n = 3$.

(E) Enrichment of *HIPK3*, *BRCA1*, and *GAPDH* (negative control) in *HIPK3 mRNA* native pull-down and control LacZ pull-down performed in RD cells. $n = 3$.

Data are represented as mean for (B) and (C), or mean of enrichment versus input (D and E) ± SD.

See also Figure S2.

luciferase signal upon *circHIPK3* or *HIPK3* mRNA depletion (Figure S2F). To exclude the possible *circHIPK3* miRNA sponging activity to regulate BRCA1 protein levels, we made a specific native RNA pull-down followed by high-throughput small RNA-seq. Using the same stringent enrichment analysis previously used for the psoralen-crosslinked pull-down, only three miRNAs were enriched: hsa-let7b-5p, hsa-miR21-5p, and hsa-miR877-5p (Figure S2G; Table S2). However, validation of those targets was far from optimal; miR-877 could barely be detected and enrichment of let7b-5p and miR21-5p was low and exceedingly variable (Figure S2H). Anyhow, we tried to block the effects of those miRNAs using LNA antisense technology. As can be observed in Figures S2I and S2J, transfection of LNA blockers against miR21-5p or Let7b-5p does not alter either *circHIPK3* level or *BRCA1* mRNA but increases the mRNA levels of miR21-5p targets *CDC25A*, *TIMP3*, and *BCL2*[17–19] or Let7b-5p targets *CDC34*, *COIL*, and *CCND1*.[20,21] Moreover, *circHIPK3* depletion did not change the levels of known Let7-5p nor miR21-5p targets (Figure S2K). All these data discard the miRNA sponge effect of *circHIPK3* to regulate *BRCA1* mRNA.

The *RNA-RNA* interaction involves the back-splicing junction of *circHIPK3* and the last coding exon of *BRCA1* mRNA

We then focused on the circRNA-mRNA interaction as the primary regulatory mechanism. The IntaRNA program, which calculates the optimal free energy interacting regions of two RNAs, predicted a variegated range of pairing between *circHIPK3* and its mRNA interactors (Table S3). When we compared such predictions with a control set of random RNAs, with matched length and structure (5′ UTR, CDS and 3′ UTR), with pull-down RNAs (Figure S3A), we found that there is only one region of circHIPK3 sequence that displays a significant contacts enrichment with pull-down RNAs and that this region coincides with its BSJ (Figure S3B). Indeed, in the case of *BRCA1* mRNA, the optimal prediction is between nucleotides 5,595 and 5,634 of *BRCA1* mRNA in the last coding exon of the transcript (Ensembl: ENST00000357654.9) and nucleotides 1,068–13 of the circRNA involving the region across the BSJ (Figure 3A).

We performed electrophoretic mobility gel-shift assays (EMSA) using *in vitro*-transcribed RNAs to validate this

Please cite this article in press as: Grelloni et al., BRCA1 levels and DNA-damage response are controlled by the competitive binding of *circHIPK3* or FMRP to the *BRCA1* mRNA, Molecular Cell (2024), https://doi.org/10.1016/j.molcel.2024.09.016

CellPress
OPEN ACCESS

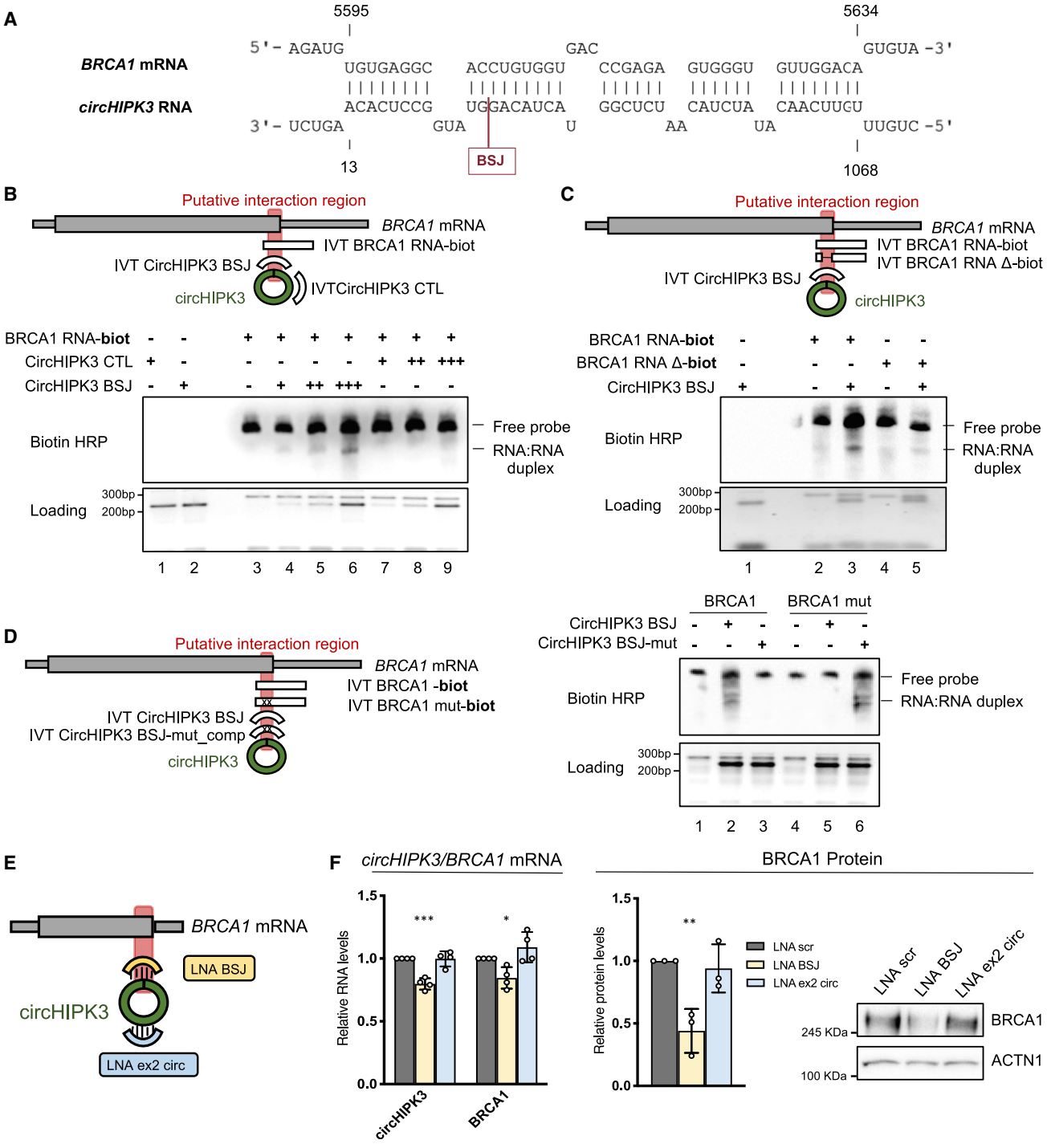

Figure 3. The RNA-RNA interaction involves the back-splicing junction of *circHIPK3* and the last coding exon of *BRCA1* mRNA

(A) circHIPK3/*BRCA1* mRNA interaction with the highest binding energy predicted by IntaRNA.

(B) Top: cartoon depicting IVT constructs. Bottom: electrophoresis mobility shift assay (EMSA) of biotinylated *in vitro*-transcribed (IVT) *BRCA1* exon-23+3′ UTR construct alone (lane 3), in increasing concentration of IVT circHIPK3-BSJ (lanes 4–6), or in increasing concentration of another IVT region of *circHIPK3*, circHIPK3-CTL (lanes 7–9).

(C) Top: cartoon depicting IVT constructs. Bottom: EMSA of biotinylated *BRCA*-exon-23+3′ UTR construct alone (lane 2) or in presence of circHIPK3-BSJ (lane 3) and of biotinylated *BRCA1*-exon-23+3′ UTR, with a deletion at the level of *circHIPK3*-predicted interaction site construct alone (lane 4), or in presence of circHIPK3-BSJ (lane 5).

(legend continued on next page)

Please cite this article in press as: Grelloni et al., BRCA1 levels and DNA-damage response are controlled by the competitive binding of *circHIPK3* or FMRP to the *BRCA1* mRNA, Molecular Cell (2024), https://doi.org/10.1016/j.molcel.2024.09.016

interaction. Incubation of a biotinylated RNA covering nucleotides 5,581–5,880 of BRCA1 (BRCA1-Ex23+3′ UTR), together with an unlabeled RNA spanning nucleotides 1,000–99 of circHIPK3-BSJ, produced a faster migrating band that was not visualized in the presence of a circHIPK3 control region (named CTL, and corresponding to nucleotides 357–562 of circHIPK3) (Figure 3B). We then performed a gel retardation assay using the biotinylated BRCA1-Ex23+3′ UTR RNA, or a mutated version lacking the predicted interaction site (biotinylated BRCA1-Ex23+3′ UTR-Δ, nucleotides 5,581–5,595/5,634–5,880), in the presence of unlabeled circHIPK3-BSJ RNA. As shown in Figure 3C, deletion of the predicted interaction site on the *BRCA1* transcript produced an almost complete abrogation of the gel-shift, confirming the importance of *BRCA1* mRNA region 5,595–5,634 as the main interaction site with *circHIPK3*. When, instead of a deletion, we substituted the interaction region with a random sequence (biotinylated BRCA1-Ex23+3′ UTR-mut), we observed a similar abrogation of the gel shift that could only be recovered when the sequence of the circHIPK3-BSJ RNA was mutated with the complementary sequence (Figures 3D and S3C). Altogether, these data show the involvement of the BSJ region of *circHIPK3* and of the selected region in *BRCA1* in the binding.

To confirm this *in vitro* interaction, we designed LNA antisense oligonucleotides to block the interaction *in vivo* between *circHIPK3* and *BRCA1* mRNA (Figure 3E). We transfected RD cells with LNA oligonucleotides against the BSJ of *circHIPK3* (LNA BSJ), a control region on the exon 2 of *HIPK3* (LNA ex2 circ) and a random control sequence (LNA scr). Only the transfection with LNA oligonucleotides against the BSJ of *circHIPK3* produced a slight downregulation of mRNA and a strong decrease in BRCA1 protein without strongly altering *circHIPK3* levels (Figure 3F). These experiments confirmed the interaction region between *circHIPK3* and *BRCA1* mRNA and the critical role of RNA-RNA interaction in regulating BRCA1 expression.

CircHIPK3 prevents FMRP binding to *BRCA1* mRNA around the interaction site

To uncover the mechanism by which *circHIPK3* regulates BRCA1 expression we searched for proteins that bind *BRCA1* mRNA by using *cat*RAPID v2.1,[22] an algorithm that computes RNA-protein interaction propensities. The analysis predicted FMRP and its paralog FXR2 as *BRCA1*-binding RBPs with the highest interaction ranking (Figure 4A). By consulting FMRP crosslinked immunoprecipitation sequencing (CLIP-seq) data,[11,23] we found several FMRP CLIP signals on *BRCA1* mRNA and, interestingly, different CLIP experiments indicate that FMRP binds a sequence on exon 23 of *BRCA1* overlapping the *circHIPK3* interacting site (Figure 4B). To deepen the mechanistic relationship between *BRCA1* mRNA, *circHIPK3*, and FMRP, we performed gel-shift assays incubating the biotinylated BRCA1-Ex23+3′ UTR RNA alternatively with unlabeled *circHIPK3*-BSJ RNA, recombinant human FRMP, or both of them together (Figures 4C and S4A). The results indicate that, with respect to the biotinylated probe alone (lane 1), incubation with circHIPK3-BSJ produced a faster migrating band (lane 2), similar to what was observed in Figure 3B, while the combination with FMRP produced a slower migrating band (lane 3). Interestingly, when the three molecules were incubated together, the band shift due to FMRP was lost while the RNA-RNA band prevailed (lane 4), indicating that the circHIPK3-BSJ RNA is able to compete *in vitro* for FMRP binding to *BRCA1* mRNA.

These data suggest a mechanism of direct competition between *circHIPK3* and FMRP for *BRCA1* mRNA binding. To perform absolute quantification of *circHIPK3* and *BRCA1* mRNA copies per cell, we established a correlation between RNA copy number and RT-qPCR efficiency using a known amount of both RNAs transcribed *in vitro*. Quantifications indicated that the RD line contains 334 copies of *circHIPK3* and 14 (13,81) copies of *BRCA1* mRNA per cell (Figure S4B). Even if we extrapolate from RNA-seq data the number of copies per cell of all other enriched mRNA interactors, we have a total of 407 molecules of mRNA interactors per RD cell, which are numbers compatible with direct competition (Figure S4C).

To test whether *circHIPK3* could regulate the binding of FMRP to *BRCA1* mRNA, we performed RNA immunoprecipitation (RIP) for FMRP in control (si-scr) and *circHIPK3*-downregulated (si-circHIPK3) RD cells. In the FMRP immunoprecipitate, we observed an enrichment of *BRCA1* mRNA but not of *circHIPK3* nor of negative controls such as *GAPDH*. Notably, in *circHIPK3*-downregulated cells we observed an increase in *BRCA1* mRNA associated with FMRP (Figures 4D and S4D). The enrichment of *GAPDH* mRNA and *HUWE1*[11] negative and positive control, respectively, did not change, indicating that the circRNA specifically regulates *BRCA1* association with FMRP. Similar results were observed with FXR2 immunoprecipitation, though with lower enrichment, possibly due to its lower expression levels in RD cells (Figure S4E).

FMRP has several binding sites along the CDS of *BRCA1 mRNA*.[11,23] To further investigate how the presence of *circHIPK3* alters the binding sites of FMRP to the mRNA, we performed CLIP in RD cells. After UV crosslinking, cells were lysed and RNA was fragmented; then, we immunoprecipitated FMRP protein in control (si-scr) and *circHIPK3*-downregulated

(D) Left: cartoon depicting IVT constructs. Right: EMSA of biotinylated *BRCA1*-exon-23+3′ UTR construct alone (lane 1), in presence of circHIPK3-BSJ (lane 2), or in presence of circHIPK3-BSJ with a mutation at the level of *BRCA1*-predicted interaction site (lane 3); EMSA of biotinylated *BRCA1*-exon-23+3′ UTR with a mutation at the level of *circHIPK3*-predicted interaction site (complementary with the one present in *circHIPK3*-BSJ-mut construct) alone (lane 4), in presence of circHIPK3-BSJ (lane 5), or in presence of circHIPK3-BSJ-mut (lane 6).

(E) Schematic representation of LNAs targeting *circHIPK3* on the *BRCA1*-binding site (LNA BSJ) or on another random sequence not predicted to interact with *BRCA1* (LNA ex2 circ).

(F) Left, RNA levels (rel. to *GAPDH*) of *circHIPK3* and *BRCA1* mRNA in RD cells transfected with LNA scr, LNA-BSJ (*circHIPK3* $p = 0.0001$; *BRCA1* $p = 0.0110$), or LNA ex2 circ. $n > 3$. Right, protein quantification (rel. to actinin) and representative western blot of BRCA1 in RD cells transfected with LNA scr, LNA BSJ ($p = 0.0053$), or LNA ex2 circ. Data are represented as mean of fold change ± SD. $n = 3$.

See also Figure S3.

Please cite this article in press as: Grelloni et al., BRCA1 levels and DNA-damage response are controlled by the competitive binding of *circHIPK3* or FMRP to the *BRCA1* mRNA, Molecular Cell (2024), https://doi.org/10.1016/j.molcel.2024.09.016

CellPress
OPEN ACCESS

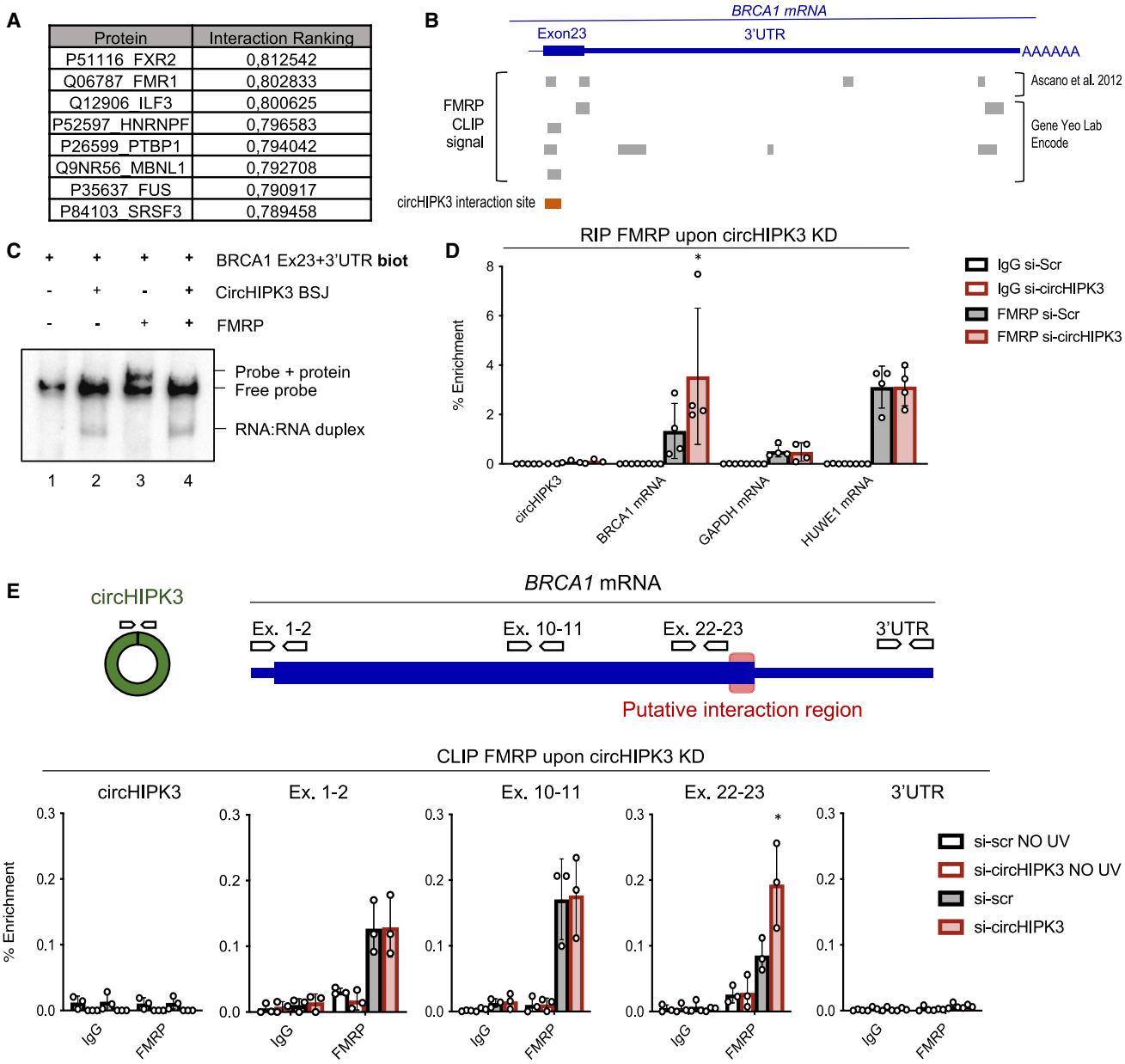

Figure 4. *CircHIPK3* prevents FMRP binding to *BRCA1* mRNA around the interaction site

(A) Table showing RBPs with the highest interaction energy with *BRCA1* mRNA according to CatRapid predictions.

(B) Integrative Genomics Viewer (IGV) reads from FMRP-CLIP (gray) from Ascano et al.[11] and Gene Yeo Lab Encode on *BRCA1* mRNA exon-23 and 3′ UTR. In orange, *circHIPK3*-binding site on *BRCA1* mRNA.

(C) EMSA of biotinylated *BRCA1*-exon-23+3′ UTR construct alone (lane 1), in the presence of circHIPK3-BSJ (lane 2), in the presence of human recombinant FMRP protein (lane 3), or in the presence of both circHIPK3-BSJ and FMRP (lane 4).

(D) Enrichment of *circHIPK3*, *BRCA1* mRNA, *GAPDH* mRNA, and *HUWE1* mRNA in FMRP and IgG RIP assay performed in RD cells in si-scr or si-circHIPK3 (*BRCA1*, $p = 0.0236$) conditions. $n = 4$.

(E) Enrichment of *circHIPK3* and four different regions of *BRCA1* mRNA (Ex.1-2, Ex.10-11, Ex. 22–23, 3′ UTR), in FMRP and IgG immunoprecipitation assay performed, after RNA fragmentation, in si-scr or si-circHIPK3 ($p = 0.044$ for ex.22–23) RD cells, in NO UV and UV (CLIP) conditions. $n = 3$. The cartoon shows the oligonucleotides used to amplify *circHIPK3* and *BRCA1* regions.

For (D) and (E), data are shown as mean of enrichment versus input ± SD.

See also Figure S4.

(si-circHIPK3) RD cells. As additional controls, we also used non-crosslinked samples. Analysis of the enriched RNA confirmed again that FMRP is not binding *circHIPK3* (Figures 4E and S4F). On the other hand, we confirmed several FMRPs binding along the *BRCA1* CDS but not in the 3′ UTR region (discrimination of FMRP binding in the 5′ UTR was impossible due to the resolution of the fragmentation). Notably, in *circHIPK3*-depleted cells, we observed an increase in *BRCA1* mRNA associated with FMRP only in the region around the *circHIPK3* interaction site (Exon 22–23) but not in other binding sites along the CDS (Figures 4E and S4F).

CircHIPK3-FMRP competition regulates BRCA1 translation

To study the effects of FMRP/FXR2 binding on BRCA1 expression, we tested two siRNAs, one targeting FXR2 and the other FMRP, and we observed that either one alone induced a mild reduction in FMRP protein. In comparison, the most robust downregulation of the FMRP protein (around 73%) was obtained with the combination of the two siRNAs (si-FXR2+si-FMRP) (Figures S5A and S5B). In FMRP-downregulated (si-FXR2+si-FMRP) cells, we detected a significant increase in BRCA1 at RNA and protein levels (Figures 5A and 5B), with only a subtle effect on the levels of nascent BRCA1 pre-mRNA (Figure S5C). Altogether, these data indicate that FMRP/FXR2 negatively control BRCA1, mainly at the post-transcriptional level. In line with these results, published datasets show an increase in *BRCA1 mRNA* upon FMRP1 deletion.[24–26] Interestingly, we observed an increase in BRCA1 protein levels in other cell types (MCF7 and A172) treated with the same siRNAs (Figure S5D). Finally, we further reinforced the proposed model by observing a rescue of BRCA1 RNA and protein levels in si-circHIPK3 RD cells after the downregulation of FMRP (si-circHIPK3+si-FXR2+si-FMRP) (Figures 5C and S5E).

Among its roles in mRNA splicing, mRNA stability, and transport,[27–30] FMRP is known to act as a regulator of mRNA translation[11,25,31]; therefore, we explored whether the translation of *BRCA1* mRNA was controlled by FMRP, using two different approaches. The first made use of a Ribo-Tag approach. We transfected RD cells with a flagged ribosomal protein (60S ribosomal protein L22; RPL22) and performed tag immunoprecipitation to test *BRCA1* mRNA association to ribosomes. We observed that the KD of *circHIPK3* reduced the association of *BRCA1* mRNA to ribosomes (Figures 5D and S5F), while the downregulation of FMRP promoted the opposite effect (Figures 5E and S5G). Data are represented as percentages of input RNA, compensating for possible differences in RNA among the different conditions. The association of *GAPDH* (positive control) to flagged-RPL22 did not change in the two conditions. A second approach consisted of polysome fractionations. Upon *circHIPK3* depletion, analysis revealed a reduced association of *BRCA1* mRNA with polysomes and increased association to the ribosomal subunits and monosome fractions (Figures 5F and S5H). Conversely, when FMRP was depleted, we observed an increased association with polysomes and a reduction in the ribosomal subunits and monosome fractions (Figures 5G and S5I). The association of *ACTN1 mRNA* (positive control) to the different fractions did not significantly change in the different conditions.

Altogether, these data support the finding that *circHIPK3* competes with FMRP protein for *BRCA1* mRNA binding, and the imbalance of this competition gatekeeps the final BRCA1 productive translation. Because we have observed that, in the absence of *circHIPK3*, the *BRCA1* mRNA displays a certain level of destabilization, we cannot exclude that, besides translational regulation, there could also be an effect of FMRP at the level of RNA stability.

BRCA1 depletion through *circHIPK3* downregulation promotes DNA damage and sensitizes RD cells to DNA-damage-inducing agents

BRCA1 functions in several crucial cellular pathways that preserve genome stability, including DNA-damage-induced cell-cycle checkpoint activation, DNA-damage repair, chromatin remodeling, transcriptional regulation, and apoptosis, and its mutation is linked to hereditary breast and ovarian cancer syndrome (HBOC).[32] According to the AACR Project GENIE, only 1.59% of rhabdomyosarcoma tumors present mutations in the BRCA1 gene.[33,34] Moreover, the Integrated Rhabdomyosarcoma database of the St. Jude Children's Research Hospital shows an increase of BRCA1 protein in root mean square (RMS) samples in comparison with myoblast or myotubes (Figure S6A). We also found a similar increase when analyzing the BRCA1 mRNA and protein levels in our RMS cell lines RH4 and RD compared with myoblasts (Figure S6B), pointing out that, as in the case of *circHIPK3*, BRCA1 is upregulated in rhabdomyosarcoma.

Based on BRCA1 downregulation in RD cells upon *circHIPK3* KD, we decided to investigate whether *circHIPK3* depletion also produced DNA repair alterations. Upon *circHIPK3* KD, we detected an accumulation of DNA damage in RD cells by comet assay; notably, this increase was reversed when the BRCA1 protein was rescued by overexpression (Figures 6A and S6C). We also observed an increase in the DNA-damage-marker γ-H2AX protein levels, both by western blot (Figure 6B) and immunofluorescence (Figure 6C). Notably, no alterations in DNA damage were observed upon depletion of the linear *HIPK3* mRNA (Figure S6D).

To dissect which DNA-damage-repair pathway is affected upon circHIPK3 KD, we took advantage of two established reporter cellular systems: U2OS DR-GFP[35] (specific for homologous recombination; HR) and U2OS EJ5-GFP[36] (specific for non-homologous end-joining; NHEJ). In both systems, the repair of a site-specific double-strand break generated by the SceI meganuclease results in the restoration of a functional GFP gene. We first confirmed that the downregulation of circHIPK3 also produced the downregulation of BRCA1 in the U2OS cell line (70% reduction, Figure S6E). We then measured GFP levels by fluorescence-activated cell sorting (FACS) in U2OS DR-GFP after SceI expression, observing that circHIPK3 KD produced a decrease in GFP production, quite nicely paralleling the observed reduction in BRCA1 levels (Figure 6D). These data support that circHIPK3 acts on the HR pathway, likely through BRCA1 downregulation. Testing the NHEJ, we found reproducible, though lower, GFP production after circHIPK3 downregulation. As control, the BRCA1 KD did not produce any alteration (Figure 6E), in line with what was shown for the involvement of this protein in the NHEJ in U2OS cells.[37] These data allowed us to conclude that circHIPK3 is also affecting the NHEJ pathway, to a minor extent, through a mechanism independent from BRCA1.

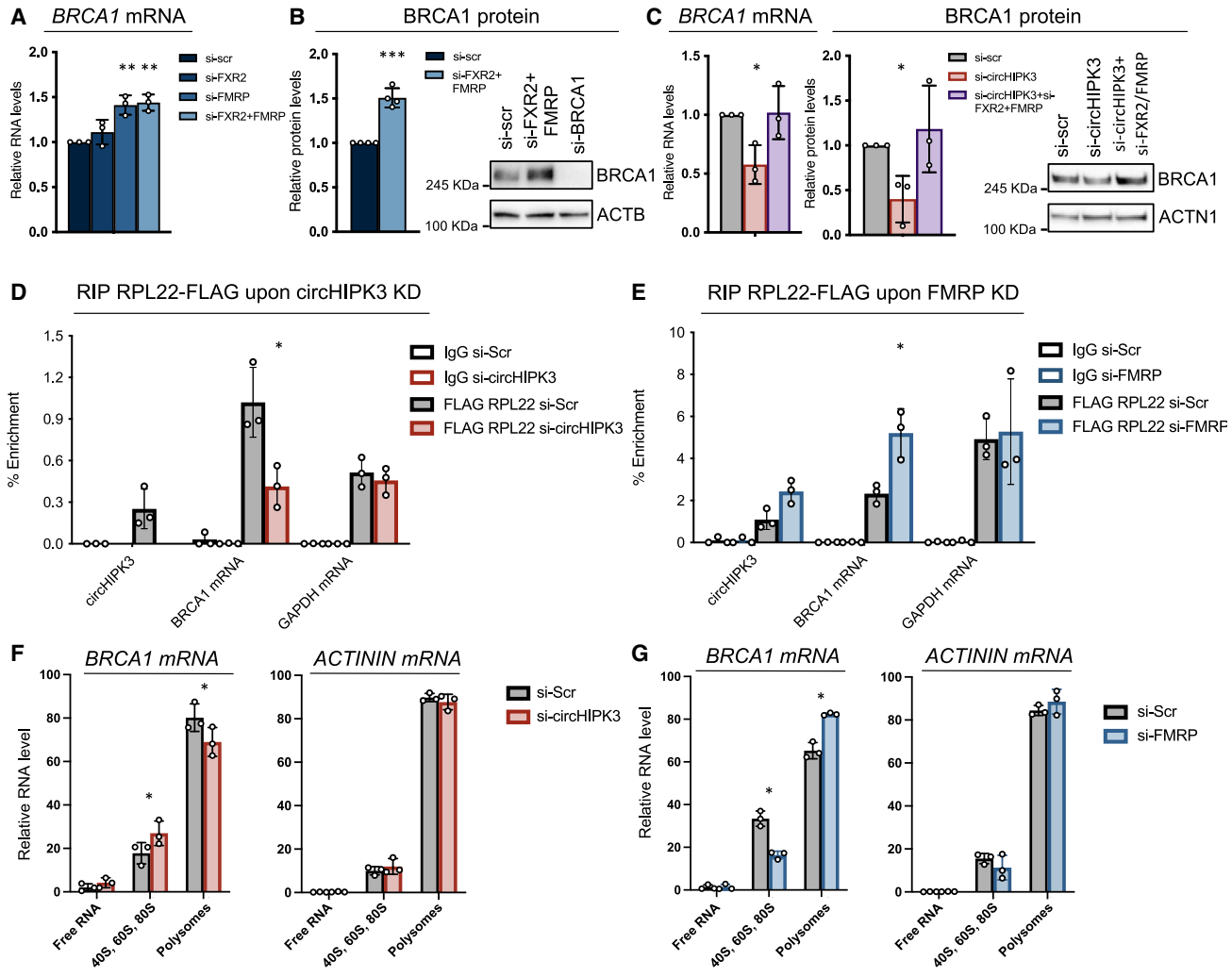

Figure 5. *CircHIPK3*-FMRP competition regulates BRCA1 translation

(A) RNA levels (rel. to *GAPDH*) measured of *BRCA1* mRNA in RD cells in si-scr, si-FXR2, si-FMRP ($p = 0.0027$), and si-FXR2+FMRP ($p = 0.0011$) conditions. $n = 3$.

(B) Protein quantification (rel. to ACTB) and representative western blot of BRCA1 in RD cells in si-scr and si-FXR2+FMRP ($p = 0.0027$) conditions. $n = 4$.

(C) Left, RNA levels (rel. to *GAPDH*) of *BRCA1* mRNA in RD cells in si-scr, si-circHIPK3 ($p = 0.0114$), and si-circHIPK3+si-FXR2+FMRP conditions. Right, protein quantification (rel. to ACTININ) and representative western blot of BRCA1 protein in RD cells in si-scr, si-circHIPK3 ($p = 0.0162$), and si-circHIPK3+si-FXR2+-FMRP conditions. $n = 3$.

(D and E) Enrichment of *circHIPK3*, *BRCA1* mRNA, and *GAPDH* mRNA in RPL22-FLAG and IgG RIP assay performed in RD cells in si-scr/si-circHIPK3 (*BRCA1* $p = 0.020$) conditions (D) or si-scr/si-FXR2+FMRP (*BRCA1* $p = 0.0449$) conditions (E). $n = 3$.

(F and G) Enrichment of *BRCA1* mRNA and *ACTININ* mRNA free, associated to ribosome subunits and monosomes, or to polysomes in si-scr/si-circHIPK3 (*BRCA1* polysomes $p = 0.028$, monosomes = 0.034) conditions (F), or si-scr/si-FXR2+FMRP (BRCA1 polysomes $p = 0.016$, monosomes = 0.016) conditions (G). Data are represented as mean of fold changes (A–C) or of enrichment versus input (D and E) ± SD. For polysomes fractionation (F and G), data are represented as percentage of RNA related to total RNA.

See also Figure S5.

Induction of DNA damage, with compounds such as cisplatin (CDDP) and doxorubicin (Dox), entails one of the most well-established strategies for cancer therapies and is based on the direct or indirect promotion of DNA lesions to override the DDR.[38,39]

Considering the BRCA1 downregulation in si-circHIPK3 RD cells, we hypothesized that the KD of *circHIPK3* could make cancer cells more sensitive to the effects of DNA-damage-inducing drugs. We detected a reduced relative survival rate in si-circHIPK3 cells treated with CDDP or DOX compared with si-scr-treated cells (Figures 6F, 6G, S6F, and S6G) and an increased apoptosis as measured by the detection of cleaved poly (ADP-ribose) polymerase 1 (PARP1) protein.[40,41]

A recent approach to tackle cancer cells is the induction of synthetic lethality in BRCA1/2-deficient cells.[42] These cells become hyper-dependent on other DNA-damage-repair-mechanism pathways, such as the one exerted by PARP1.[43,44] The inhibition of PARP1 results only lethal in BRCA1/2-defective cells,

Please cite this article in press as: Grelloni et al., BRCA1 levels and DNA-damage response are controlled by the competitive binding of *circHIPK3* or FMRP to the *BRCA1* mRNA, Molecular Cell (2024), https://doi.org/10.1016/j.molcel.2024.09.016

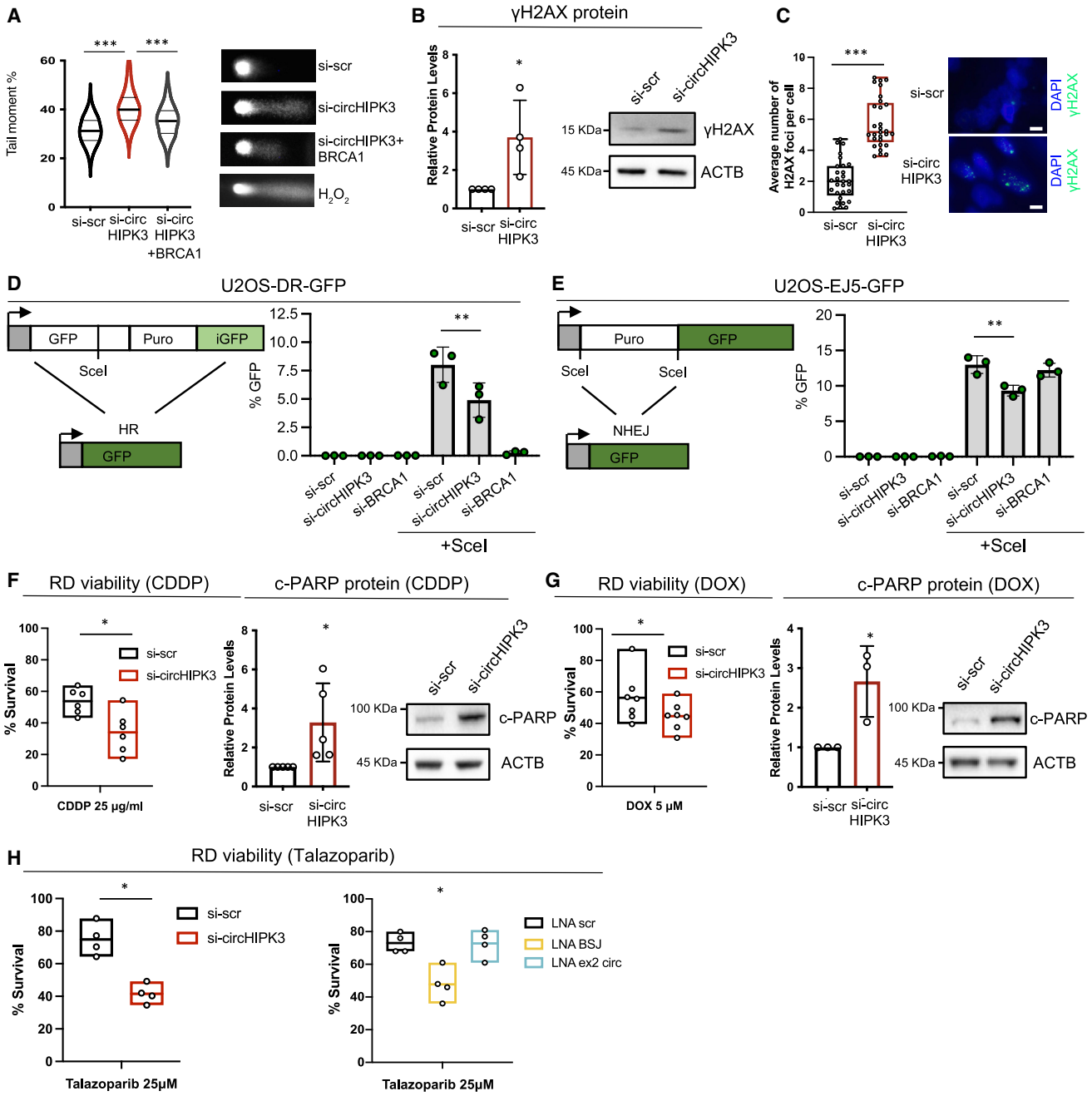

Figure 6. BRCA1 depletion through *circHIPK3* downregulation promotes DNA damage and sensitizes RD cell to DNA-damage-inducing agents

(A) Representative COMET images and quantification of the tail moment in the comet assay in si-scr and si-circHIPK3 ($p < 0.0001$) and si-circHIPK3+pc-BRCA1 ($p < 0.0001$) conditions. $n = 3$.

(B) Representative western blot and protein quantification (rel. to ACTB) of γH2AX in RD cells in si-scr and si-circHIPK3 conditions ($p = 0.0311$). $n = 4$.

(C) Representative immunofluorescence images of γH2AX (green) merged with DAPI (blue) in si-scr and si-circHIPK3 ($p < 0.0001$) conditions and quantification of γH2AX foci per cell. $n = 3$.

(D and E) Left, cartoon depicting the reporter construct to detect HR in U2OS-DR GFP (D) and NHEJ in U2OS-EJ5 GFP. Right, percentage of GFP-positive cells in si-scr, si-circHIPK3 ($p = 0.005$ and $p = 0.007$), and si-BRCA1 conditions in non-transfected and SceI-transfected cells. $n = 3$.

(F) Left, boxplots representing the percentage of survival of si-scr (black) or si-circHIPK3 (red) ($p = 0.0107$) RD cells treated for 24 h with cisplatin (CDDP). $n > 3$. Right, representative western blot and protein quantification (rel. to ACTB) of cleaved-PARP in si-scr and si-circHIPK3 ($p = 0.0339$) RD cells treated for 24 h with cisplatin (CDDP). $n > 3$.

(legend continued on next page)

Please cite this article in press as: Grelloni et al., BRCA1 levels and DNA-damage response are controlled by the competitive binding of *circHIPK3* or FMRP to the *BRCA1* mRNA, Molecular Cell (2024), https://doi.org/10.1016/j.molcel.2024.09.016

which cannot repair double-strand breaks through HR,[45] and not in healthy tissues. As shown in Figure 6H (left), si-scr RD cells treated with talazoparib, a PARP inhibitor already in clinical use, showed a mean 74.9% survival rate compared with non-treated cells, while the percentage of survived si-*circHIPK3* RD cells after the treatment resulted in 41.5%. Moreover, only the use of LNA oligonucleotides to disrupt the interaction between *circHIPK3* and *BRCA1* mRNA (LNA BSJ) led to an increase in talazoparib sensitivity (Figure 6H, right). These data indicate that the downregulation of *circHIPK3*, or the disruption of the *circHIPK3-BRCA1* mRNA interaction, causes a reduction in BRCA1 levels and might sensitize BRCA1 wild-type cancer cells to PARP inhibitors, expanding the types of tumors that could be treated with these drugs.

CircHIPK3 regulates *BRCA1* mRNA in several cancer cell lines, and the interaction might revert the BRCA1-deficiency phenotype in breast HBOC cell models

CircHIPK3 levels are upregulated in several cancer types[5–9]; therefore, we wondered whether *circHIPK3*-mediated BRCA1 regulation also existed in other cancer cell types. As in the case of Rhabdomyosarcoma, BRCA1 is only spuriously mutated in other cancer cell types. According to AACR Project GENIE, only 3% of cases in pan-cancer studies (4,966/167,224) contain a mutation in the BRCA1 sequence.[33,34] Upon analyzing the expression levels of *BRCA1* mRNA from the TCGA and GENT2[46] database projects, which contain a large amount of expression data from patients, we observed that *BRCA1* mRNA was upregulated in various cancer types compared with healthy tissues (Figure S7A). Interestingly, *circHIPK3* is upregulated in most of these cancer types.[5–9] Notably, FMRP is expressed in all tissues, so our regulation model would be easily exportable to other cancer types.

To validate the model in other cancers, we selected several cell lines representing various tumors and performed part of the experimental set we used to validate our rhabdomyosarcoma model. Using A172 cells as a model of glioblastoma, or SKOV-3 cells as a model of ovarian adenocarcinoma, we observed conservation of the interaction in the RNA pull-down between *circHIPK3* and *BRCA1* mRNA, a decrease in BRCA1 protein upon *circHIPK3* depletion, increased sensitivity to CDDP, and induction to synthetic lethality with talazoparib (Figures 7A, 7B, S7B, and S7C). We also tested other cell models, such as lung epithelial carcinoma cells A549, where similar results were obtained (Figure S7D). Similar results were also observed in non-cancerous cell lines such as myoblast (Figure S7E).

Finally, we moved to a breast ductal carcinoma model using MCF7 cells. In this cell line, we were able to observe: (1) the *circHIPK3-BRCA1* mRNA interaction in the RNA pull-down; (2) BRCA1 protein downregulation upon *circHIPK3* depletion, which was not paralleled by *HIPK3* mRNA KD; (3) increased sensitivity to DNA-damage-inducing drugs; and (4) induction of synthetic lethality after talazoparib treatment (Figure 7C). All these data helped us confirm our regulatory model as a possible pan-cancer general mechanism to control BRCA1 levels.

To test whether the correlation between *circHIPK3* and *BRCA1* mRNA was causal, we moved to a model of BRCA1 haploinsufficiency. We used an MCF7 BRCA1 hemizygous cell line, namely wt/del (clone 5–9), obtained by CRISPR-Cas9-induced large deletions of the entire coding region of the BRCA1 gene, leaving only one intact allele (Figures S7F and S7G). As observed in Figures 7D and S7H, this deficiency produces a decrease in BRCA1 protein and RNA levels. When we transfect those cells with LNA oligonucleotides corresponding to the BSJ region of *circHIPK3* (LNAex23), thus mimicking the competition of *circHIPK3* for the FMRP-binding site, we observed an increase in BRCA1 levels in wt/wt cells but also a restoration of BRCA1 levels in hemizygous wt/del cells, making them similar to wild-type cells.

Remarkably, DNA damage levels of those cells mirror the levels of BRCA protein, making the DDR in MCF7 wt/del cells transfected with the LNA Ex23 comparable with the response in MCF7 wt/wt cells (Figure 7D, right).

This last experiment supports the functional correlation between the levels of *circHIPK3* and those of the BRCA1 protein and opens the intriguing therapeutic possibility of reverting the hereditary breast cancer syndrome produced by BRCA1 mutations.

DISCUSSION

Many studies in the past described the function of circRNAs as miRNA sponges and, through such activity, their deregulation has been associated with several pathological processes, especially cancer. A paradigmatic example is represented by *circHIPK3*, a circRNA upregulated in a myriad of tumors[5–9] and that has been attributed a role of competing endogenous RNA (ceRNA) in many cancers, with the ability to sponge different miRNAs in diverse systems. Here, using psoralen crosslinking, which is the gold standard to detect RNA-RNA interactions *in vivo*, we have shown a different mechanism of the *circHIPK3* mode of action based on its ability to interact with specific mRNAs.

We found and validated a noteworthy pairing between *circHIPK3* and the *BRCA1* mRNA. The involvement of the BSJ region of *circHIPK3* in the interaction makes this binding specific for the circRNA and not for the linear counterpart. Due to the lack of homology with *BRCA2* mRNA, this interaction is restricted to *BRCA1*. Notably, we found that such interaction competes for the binding of FMRP in a specific region of the *BRCA1* mRNA. Absolute quantifications of the copy number per cell of both

(G) Left, boxplots representing the percentage of survival of si-scr (black) or si-circHIPK3 (red) ($p = 0.0231$) RD cells treated for 24 h with doxorubicin (DOX). $n > 3$. Right, representative western blot and protein quantification (rel. to ACTB) of cleaved-PARP in si-scr and si-circHIPK3 ($p = 0.0325$) RD cells treated for 24 h with doxorubicin (DOX). $n = 3$.

(H) Left, boxplots representing the percentage of survival of si-scr (black) or si-circHIPK3 (red) ($p = 0.0211$) RD cells treated for 24 h with talazoparib. $n = 4$. Right, boxplots representing the percentage of survival of LNA-scr (black), LNA-BSJ (yellow) ($p = 0.0256$), and LNA-ex2-circ (cyan) transfected RD cells treated for 24 h with talazoparib. $n > 3$.

Data are represented as mean of relative protein levels in (B), (F) right, and (G) right, ± SD.

See also Figure S6.

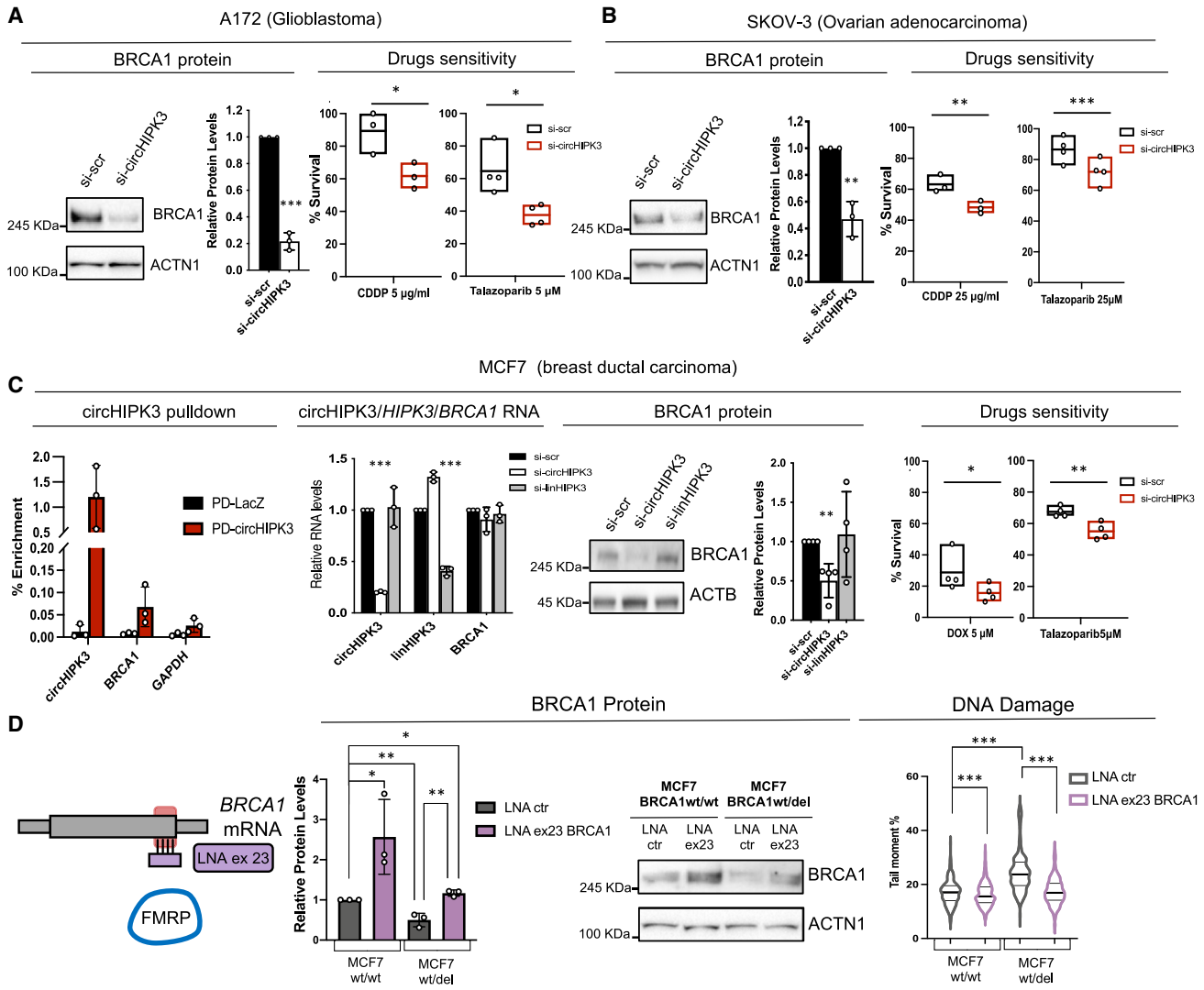

Figure 7. *CircHIPK3* regulates *BRCA1* mRNA in several cancer cell lines, and the interaction might revert the BRCA1-deficiency phenotype in breast HBOC cell models

(A) Left, protein quantification (rel. to ACTININ) and representative western blot of BRCA1 in si-scr and si-circHIPK3 ($p < 0.0001$) A172 cells. $n = 3$. Right, boxplots representing the survival percentage of si-scr (black) or si-circHIPK3 (red) (CDDP $p = 0.0146$; Tal $p = 0.0144$) A172 cells treated for 48 h with cisplatin (CDDP) or talazoparib. $n \geq 3$.

(B) Left, protein quantification (rel. to ACTININ) and representative western blot of BRCA1 in si-scr and si-circHIPK3 ($p = 0.0022$) SKOV-3 cells. $n = 3$. Right, boxplots representing the survival percentage of si-scr (black) or si-circHIPK3 (red) (CDDP $p = 0.0053$; Tal $p = 0.0008$) SKOV-3 cells treated for 24 h with cisplatin (CDDP) or 30 h with talazoparib. $n \geq 3$.

(C) Left, RT-qPCR showing the enrichment of *circHIPK3*, *BRCA1*, and *GAPDH* mRNA in circHIPK3 native pull-down and control LacZ pull-down in MCF7 cells. $n = 3$. Middle, RNA levels (rel. to *GAPDH*) of *circHIPK3*, *HIPK3*, and *BRCA1* mRNA in si-scr, si-circHIPK3 (circHIPK3 $p < 0001$), and si-linHIPK3 MCF7 cells (*HIPK3* $p < 0001$); protein quantification (rel. to ACTB) and representative western blot of BRCA1 in si-scr, si-circHIPK3 ($p = 0.035$), and si-linHIPK3 MCF7 cells. $n > 3$. Right, boxplots representing the survival percentage of si-scr (black) or si-circHIPK3 (red) (DOX $p = 0.0382$; Tal $p = 0.0015$) MCF7 cells treated for 24 h with doxorubicin (DOX) or 48 h with talazoparib. $n > 3$.

(D) Left, schematic representation of the LNA targeting *BRCA1* on the FMRP-binding site (LNA ex23). Middle, protein quantification (rel. to ACTININ) and representative western blot of BRCA1 in wt/wt and wt/del MCF7 cells transfected with LNA ctr or LNA ex23 (wt/wt ctr versus wt/wt ex23 $p = 0.0433$; wt/wt ctr versus wt/del ctr $p = 0.0068$; wt/del ctr versus wt/del ex23 $p = 0.0033$; wt/wt ctr versus wt/del ex23 $p = 0.0196$). $n = 3$. Right, quantification of the tail moment in the comet assay in wt/wt and wt/del MCF7 cells transfected with LNA ctr or LNA ex23 (wt/wt ctr versus wt/wt ex23 $p = 0.0002$; wt/wt ctr versus wt/del ctr $p \leq 0.0001$; wt/del ctr versus wt/del ex23 $p \leq 0.0001$). $n = 3$.

Data are represented as mean of fold changes (RNA and protein quantification) or of enrichment versus input (for RNA pull-down) ± SD.

See also Figure S7.

RNAs justifies this competitive model. Our data indicated that, in the absence of *circHIPK3*, FMRP efficiently operates its repression on *BRCA1* mRNA translation and, possibly, stability, while in the presence of *circHIPK3*, the competition for FMRP binding alleviates such repression. The association of *circHIPK3* with the ribosomal subunit fractions would indicate that the interaction with the *BRCA1* mRNA is released upon loading of the mRNA onto polysomes.

BRCA1 has a crucial role in homology recombination repair after DNA damage, and its partial or total abrogation is associated with different cancer onsets, as occurs in the case of the hereditary breast and ovarian cancer syndrome. BRCA1 is a classic tumor-suppressor gene, and its mutation is severely linked to cancer. However, analysis of a large amount of sequencing data indicated that BRCA1 is overexpressed as a wild-type form in many cancers. This counterintuitive overexpression of *BRCA1* mRNA in tumor samples described in our data, and also present in the literature,[47–53] should not be interpreted as an oncogenic feature of BRCA1 but as an adaptative cellular response to cope with increased cellular damage present in cancer cells and to avoid DNA-damage-induced apoptosis.

Thus, the ability of *circHIPK3* to regulate BRCA1 levels implies controlling the balance between DNA damage and DNA repair. The *circHIPK3* capability to modulate BRCA1 levels opens exciting therapeutical possibilities, both in the case of BRCA1 haploinsufficiency and of upregulation.

Our data demonstrate that using siRNAs against *circHIPK3* RNA or LNA-modified oligonucleotides against its BSJ, which prevent *circHIPK3-BRCA1* mRNA interaction, could represent a possible adjuvant therapy to prevent tumor growth. On the other hand, LNA oligonucleotides, which compete with FMRP binding on the *BRCA1* mRNA, led to an increase in BRCA1 protein and restored its physiological levels in cells hemizygous for BRCA1, such as in the hereditary breast and ovarian cancer syndrome.

Despite the significant challenges in developing RNA-based therapeutics, several RNA-based medications have been approved or are undergoing clinical trials.[54,55] Understanding the ncRNA functions and their crucial roles in disease development is critical to broadening the potential therapeutic target pool. Disrupting mRNA-circRNA interactions might represent a powerful strategy to alter cell homeostasis and open an approach to tackle pathologies such as cancer.

Limitations of the study

We have restricted the analysis to the effect of *circHIPK3* on the BRCA1 factor because of its important role in the control of the DDR. In parallel, circHIPK3 might be regulating other mRNA that might be contributing to the DNA-damage phenotype together with BRCA1 downregulation. Similarly, we cannot exclude that, besides FMRP, additional factors could concur with the described regulatory process for *BRCA1* mRNA.

RESOURCE AVAILABILITY

Lead contact

Further information and requests for resources and reagents should be directed to and will be fulfilled by the lead contact, Irene Bozzoni (irene.bozzoni@uniroma1.it).

Materials availability

All unique/stable reagents generated in this study are available from the lead contact upon request.

Data and code availability

- RNA-seq data from RNA pull-down experiments have been deposited at Gene Expression Omnibus GEO: GSE246226 and uncropped images and blots and FACS have been deposited to Mendeley database repository (DOI: https://doi.org/10.17632/fk8bm3rxh2.1) and are publicly available as of the date of publication. The accession number of other databases used in article are listed in the key resources table.
- This paper does not report original code.
- Any additional information required to reanalyze the data reported in this paper is available from the lead contact upon request.

ACKNOWLEDGMENTS

We thank Prof. Fatica, Dr. Bagnato, Dr. Monteonofrio, Dr. Soddu, Dr. Megiorni, Dr. Dominici, Dr. Gunn, Dr. Stark, and Dr. Oberdoerffer for cells and reagents. We thank Dr. Vozzi and the Genomic Facility of IIT for support in RNA-seq. We are especially grateful to Dr. Gioia and Prof. D'Adda Di Fagagna for providing expertise and advice in the DNA-damage experiments. We are also grateful to M. Marchioni, A. Pierri, and M. Guarnacci for technical help and to Dr Caruso for assistance. This work is dedicated to the memory of Prof. Francesco Amaldi, who founded the lab and whose scientific and teaching legacies will forever remain a great example. This work was supported by grants from AIRC (IG 2019 Id.23053), ERC ERC-2019-SyG 855923-ASTRA, and MUR "National Center for Gene Therapy and Drugbased on RNA Technology and NextGenerationEU PNRR MUR(CN00000041).

AUTHOR CONTRIBUTIONS

C.G. and M.B. co-designed and performed most of the experiments. A.S. performed bioinformatical analyses, and G.P. performed FACS. R.G. and F.R. helped in the experimental part. M.C., M.C.D.R., and M.A.P. generated hemizygous MCF7 cells. C.G., M.B., and I.B. wrote the manuscript with inputs from all the authors. M.B. and I.B. co-designed, supervised, and coordinated the work.

DECLARATION OF INTERESTS

The authors declare no competing interests.

STAR★METHODS

Detailed methods are provided in the online version of this paper and include the following:

- KEY RESOURCES TABLE
- EXPERIMENTAL MODEL AND STUDY PARTICIPANT DETAILS
  - Cell cultures
  - Patient biopsies
- METHOD DETAILS
  - Plasmid construction
  - Rnase R treatment
  - Cell transfection
  - sgRNAs, ssODN, and primers
  - CRISPR/Cas9-mediated generation of BRCA1 hemizygous MCF7 cells
  - Western blot
  - RNA isolation and analysis
  - RNA pull down
  - RNA immunoprecipitation
  - Drug treatment
  - Polysome fractionation
  - Immunofluorescence

SUPPLEMENTAL INFORMATION

Supplemental information can be found online at https://doi.org/10.1016/j.molcel.2024.09.016.

Received: November 7, 2023
Revised: August 22, 2024
Accepted: September 13, 2024
Published: October 9, 2024

REFERENCES

1. Statello, L., Guo, C.-J., Chen, L.-L., and Huarte, M. (2021). Gene regulation by long non-coding RNAs and its biological functions. Nat. Rev. Mol. Cell Biol. *22*, 96–118. https://doi.org/10.1038/s41580-020-00315-9.
2. Fatica, A., and Bozzoni, I. (2014). Long non-coding RNAs: new players in cell differentiation and development. Nat. Rev. Genet. *15*, 7–21. https://doi.org/10.1038/nrg3606.
3. Guarnerio, J., Bezzi, M., Jeong, J.C., Paffenholz, S.V., Berry, K., Naldini, M.M., Lo-Coco, F., Tay, Y., Beck, A.H., and Pandolfi, P.P. (2016). Oncogenic Role of Fusion-circRNAs Derived from Cancer-Associated Chromosomal Translocations. Cell *165*, 289–302. https://doi.org/10.1016/j.cell.2016.03.020.
4. Patop, I.L., and Kadener, S. (2018). circRNAs in cancer. Curr. Opin. Genet. Dev. *48*, 121–127. https://doi.org/10.1016/J.GDE.2017.11.007.
5. Li, Y., Zheng, F., Xiao, X., Xie, F., Tao, D., Huang, C., Liu, D., Wang, M., Wang, L., Zeng, F., and Jiang, G. (2017). CircHIPK3 sponges miR-558 to suppress heparanase expression in bladder cancer cells. EMBO Rep. *18*, 1646–1659. https://doi.org/10.15252/embr.201643581.
6. Zheng, Q., Bao, C., Guo, W., Li, S., Chen, J., Chen, B., Luo, Y., Lyu, D., Li, Y., Shi, G., et al. (2016). Circular RNA profiling reveals an abundant circHIPK3 that regulates cell growth by sponging multiple miRNAs. Nat. Commun. *7*, 11215. https://doi.org/10.1038/ncomms11215.
7. Chen, G., Shi, Y., Liu, M., and Sun, J. (2018). circHIPK3 regulates cell proliferation and migration by sponging miR-124 and regulating AQP3 expression in hepatocellular carcinoma. Cell Death Dis. *9*, 175. https://doi.org/10.1038/s41419-017-0204-3.
8. Chen, Z.G., Zhao, H.J., Lin, L., Liu, J.B., Bai, J.Z., and Wang, G.S. (2020). Circular RNA CirCHIPK3 promotes cell proliferation and invasion of breast cancer by sponging miR-193a/ HMGB1/PI3K/AKT axis. Thorac. Cancer *11*, 2660–2671. https://doi.org/10.1111/1759-7714.13603.
9. Teng, F., Xu, J., Zhang, M., Liu, S., Gu, Y., Zhang, M., Wang, X., Ni, J., Qian, B., Shen, R., and Jia, X. (2019). Comprehensive circular RNA expression profiles and the tumor-suppressive function of circHIPK3 in ovarian cancer. Int. J. Biochem. Cell Biol. *112*, 8–17. https://doi.org/10.1016/j.biocel.2019.04.011.
10. Li, Z., Zhang, Y., Ku, L., Wilkinson, K.D., Warren, S.T., and Feng, Y. (2001). The fragile X mental retardation protein inhibits translation via interacting with mRNA. Nucleic Acids Res. *29*, 2276–2283. https://doi.org/10.1093/nar/29.11.2276.
11. Ascano, M., Mukherjee, N., Bandaru, P., Miller, J.B., Nusbaum, J.D., Corcoran, D.L., Langlois, C., Munschauer, M., Dewell, S., Hafner, M., et al. (2012). FMRP targets distinct mRNA sequence elements to regulate protein expression. Nature *492*, 382–386. https://doi.org/10.1038/nature11737.
12. Liu, X.S., Wu, H., Krzisch, M., Wu, X., Graef, J., Muffat, J., Hnisz, D., Li, C.H., Yuan, B., Xu, C., et al. (2018). Rescue of Fragile X Syndrome Neurons by DNA Methylation Editing of the FMR1 Gene. Cell *172*, 979–992.e6. https://doi.org/10.1016/j.cell.2018.01.012.
13. Zhang, Y.Q., Bailey, A.M., Matthies, H.J.G., Renden, R.B., Smith, M.A., Speese, S.D., Rubin, G.M., and Broadie, K. (2001). Drosophila Fragile X-Related Gene Regulates the MAP1B Homolog Futsch to Control Synaptic Structure and Function. Cell *107*, 591–603. https://doi.org/10.1016/S0092-8674(01)00589-X.
14. Zalfa, F., Eleuteri, B., Dickson, K.S., Mercaldo, V., De Rubeis, S., di Penta, A., Tabolacci, E., Chiurazzi, P., Neri, G., Grant, S.G.N., and Bagni, C. (2007). A new function for the fragile X mental retardation protein in regulation of PSD-95 mRNA stability. Nat. Neurosci. *10*, 578–587. https://doi.org/10.1038/nn1893.
15. Dattilo, D., Di Timoteo, G., Setti, A., Giuliani, A., Peruzzi, G., Beltran Nebot, M., Centrón-Broco, A., Mariani, D., Mozzetta, C., and Bozzoni, I. (2023). The m6A reader YTHDC1 and the RNA helicase DDX5 control the production of rhabdomyosarcoma-enriched circRNAs. Nat. Commun. *14*, 1898. https://doi.org/10.1038/s41467-023-37578-7.
16. Memczak, S., Jens, M., Elefsinioti, A., Torti, F., Krueger, J., Rybak, A., Maier, L., Mackowiak, S.D., Gregersen, L.H., Munschauer, M., et al. (2013). Circular RNAs are a large class of animal RNAs with regulatory potency. Nature *495*, 333–338. https://doi.org/10.1038/nature11928.
17. Wang, P., Zou, F., Zhang, X., Li, H., Dulak, A., Tomko, R.J., Lazo, J.S., Wang, Z., Zhang, L., and Yu, J. (2009). microRNA-21 negatively regulates Cdc25A and cell cycle progression in colon cancer cells. Cancer Res. *69*, 8157–8165. https://doi.org/10.1158/0008-5472.CAN-09-1996.
18. Gabriely, G., Wurdinger, T., Kesari, S., Esau, C.C., Burchard, J., Linsley, P.S., and Krichevsky, A.M. (2008). MicroRNA 21 Promotes Glioma Invasion by Targeting Matrix Metalloproteinase Regulators. Mol. Cell. Biol. *28*, 5369–5380. https://doi.org/10.1128/MCB.00479-08.
19. Sims, E.K., Lakhter, A.J., Anderson-Baucum, E., Kono, T., Tong, X., and Evans-Molina, C. (2017). MicroRNA 21 targets BCL2 mRNA to increase apoptosis in rat and human beta cells. Diabetologia *60*, 1057–1065. https://doi.org/10.1007/s00125-017-4237-z.
20. Schultz, J., Lorenz, P., Gross, G., Ibrahim, S., and Kunz, M. (2008). MicroRNA let-7b targets important cell cycle molecules in malignant melanoma cells and interferes with anchorage-independent growth. Cell Res. *18*, 549–557. https://doi.org/10.1038/cr.2008.45.
21. Legesse-Miller, A., Elemento, O., Pfau, S.J., Forman, J.J., Tavazoie, S., and Coller, H.A. (2009). let-7 Overexpression Leads to an Increased Fraction of Cells in G2/M, Direct Down-regulation of Cdc34, and Stabilization of Wee1 Kinase in Primary Fibroblasts. J. Biol. Chem. *284*, 6605–6609. https://doi.org/10.1074/jbc.C900002200.
22. Bellucci, M., Agostini, F., Masin, M., and Tartaglia, G.G. (2011). Predicting protein associations with long noncoding RNAs. Nat. Methods *8*, 444–445. https://doi.org/10.1038/nmeth.1611.
23. Van Nostrand, E.L., Freese, P., Pratt, G.A., Wang, X., Wei, X., Xiao, R., Blue, S.M., Chen, J.-Y., Cody, N.A.L., Dominguez, D., et al. (2020). A large-scale binding and functional map of human RNA-binding proteins. Nature *583*, 711–719. https://doi.org/10.1038/s41586-020-2077-3.
24. Su, S., Xue, Y., Sharov, A., Zhang, Y., Lee, S.K., Martindale, J.L., Li, W., Ku, W.L., Zhao, K., De, S., et al. (2022). A dual-activity topoisomerase complex regulates mRNA translation and turnover. Nucleic Acids Res. *50*, 7013–7033. https://doi.org/10.1093/nar/gkac538.
25. Kurosaki, T., Mitsutomi, S., Hewko, A., Akimitsu, N., and Maquat, L.E. (2022). Integrative omics indicate FMRP sequesters mRNA from translation and deadenylation in human neuronal cells. Mol. Cell *82*, 4564–4581.e11. https://doi.org/10.1016/j.molcel.2022.10.018.
26. Luo, Y., Hitz, B.C., Gabdank, I., Hilton, J.A., Kagda, M.S., Lam, B., Myers, Z., Sud, P., Jou, J., Lin, K., et al. (2020). New developments on the Encyclopedia of DNA Elements (ENCODE) data portal. Nucleic Acids Res. *48*, D882–D889. https://doi.org/10.1093/nar/gkz1062.

27. Mazroui, R., Huot, M.-E., Tremblay, S., Filion, C., Labelle, Y., and Khandjian, E.W. (2002). Trapping of messenger RNA by Fragile X Mental Retardation protein into cytoplasmic granules induces translation repression. Hum. Mol. Genet. *11*, 3007–3017. https://doi.org/10.1093/hmg/11.24.3007.

28. Antar, L.N., Li, C., Zhang, H., Carroll, R.C., and Bassell, G.J. (2006). Local functions for FMRP in axon growth cone motility and activity-dependent regulation of filopodia and spine synapses. Mol. Cell. Neurosci. *32*, 37–48. https://doi.org/10.1016/j.mcn.2006.02.001.

29. Didiot, M.-C., Tian, Z., Schaeffer, C., Subramanian, M., Mandel, J.-L., and Moine, H. (2008). The G-quartet containing FMRP binding site in FMR1 mRNA is a potent exonic splicing enhancer. Nucleic Acids Res. *36*, 4902–4912. https://doi.org/10.1093/nar/gkn472.

30. Bechara, E.G., Didiot, M.C., Melko, M., Davidovic, L., Bensaid, M., Martin, P., Castets, M., Pognonec, P., Khandjian, E.W., Moine, H., and Bardoni, B. (2009). A novel function for fragile X mental retardation protein in translational activation. PLoS Biol. *7*, e16. https://doi.org/10.1371/journal.pbio.1000016.

31. Brown, V., Jin, P., Ceman, S., Darnell, J.C., O'Donnell, W.T., Tenenbaum, S.A., Jin, X., Feng, Y., Wilkinson, K.D., Keene, J.D., et al. (2001). Microarray Identification of FMRP-Associated Brain mRNAs and Altered mRNA Translational Profiles in Fragile X Syndrome. Cell *107*, 477–487. https://doi.org/10.1016/S0092-8674(01)00568-2.

32. Wu, J., Lu, L.-Y., and Yu, X. (2010). The role of BRCA1 in DNA damage response. Protein Cell *1*, 117–123. https://doi.org/10.1007/s13238-010-0010-5.

33. de Bruijn, I., Kundra, R., Mastrogiacomo, B., Tran, T.N., Sikina, L., Mazor, T., Li, X., Ochoa, A., Zhao, G., Lai, B., et al. (2023). Analysis and Visualization of Longitudinal Genomic and Clinical Data from the AACR Project GENIE Biopharma Collaborative in cBioPortal. Cancer Res. *83*, 3861–3867. https://doi.org/10.1158/0008-5472.CAN-23-0816.

34. Cerami, E., Gao, J., Dogrusoz, U., Gross, B.E., Sumer, S.O., Aksoy, B.A., Jacobsen, A., Byrne, C.J., Heuer, M.L., Larsson, E., et al. (2012). The cBio Cancer Genomics Portal: An Open Platform for Exploring Multidimensional Cancer Genomics Data. Cancer Discov. *2*, 401–404. https://doi.org/10.1158/2159-8290.CD-12-0095.

35. Khurana, S., Kruhlak, M.J., Kim, J., Tran, A.D., Liu, J., Nyswaner, K., Shi, L., Jailwala, P., Sung, M.-H., Hakim, O., and Oberdoerffer, P. (2014). A Macrohistone Variant Links Dynamic Chromatin Compaction to BRCA1-Dependent Genome Maintenance. Cell Rep. *8*, 1049–1062. https://doi.org/10.1016/j.celrep.2014.07.024.

36. Gunn, A., and Stark, J.M. (2012). I-SceI-Based Assays to Examine Distinct Repair Outcomes of Mammalian Chromosomal Double Strand Breaks. Methods Mol Biol. *920*, 379–391. https://doi.org/10.1007/978-1-61779-998-3_27.

37. Swift, M.L., Beishline, K., Flashner, S., and Azizkhan-Clifford, J. (2021). DSB repair pathway choice is regulated by recruitment of 53BP1 through cell cycle-dependent regulation of Sp1. Cell Rep. *34*, 108840. https://doi.org/10.1016/j.celrep.2021.108840.

38. Reedijk, J., and Lohman, P.H.M. (1985). Cisplatin: synthesis, antitumour activity and mechanism of action. Pharm. Weekbl. Sci. *7*, 173–180. https://doi.org/10.1007/BF02307573.

39. Gewirtz, D.A. (1999). A critical evaluation of the mechanisms of action proposed for the antitumor effects of the anthracycline antibiotics adriamycin and daunorubicin. Biochem. Pharmacol. *57*, 727–741. https://doi.org/10.1016/S0006-2952(98)00307-4.

40. Kaufmann, S.H., Desnoyers, S., Ottaviano, Y., Davidson, N.E., and Poirier, G.G. (1993). Specific proteolytic cleavage of poly(ADP-ribose) polymerase: an early marker of chemotherapy-induced apoptosis. Cancer Res. *53*, 3976–3985.

41. Salvesen, G.S., and Dixit, V.M. (1997). Caspases: Intracellular Signaling by Proteolysis. Cell *91*, 443–446. https://doi.org/10.1016/S0092-8674(00)80430-4.

42. Ashworth, A. (2008). A Synthetic Lethal Therapeutic Approach: Poly(ADP) Ribose Polymerase Inhibitors for the Treatment of Cancers Deficient in DNA Double-Strand Break Repair. J. Clin. Oncol. *26*, 3785–3790. https://doi.org/10.1200/JCO.2008.16.0812.

43. Dantzer, F., Amé, J., Schreiber, V., Nakamura, J., Ménissier-de Murcia, J., and de Murcia, G. (2006). Poly(ADP-ribose) Polymerase–1 Activation During DNA Damage and Repair. Methods Enzymol. *409*, 493–510. https://doi.org/10.1016/S0076-6879(05)09029-4.

44. Haber, J.E. (1999). DNA recombination: the replication connection. Trends Biochem. Sci. *24*, 271–275. https://doi.org/10.1016/S0968-0004(99)01413-9.

45. Farmer, H., McCabe, N., Lord, C.J., Tutt, A.N.J., Johnson, D.A., Richardson, T.B., Santarosa, M., Dillon, K.J., Hickson, I., Knights, C., et al. (2005). Targeting the DNA repair defect in BRCA mutant cells as a therapeutic strategy. Nature *434*, 917–921. https://doi.org/10.1038/nature03445.

46. Park, S.-J., Yoon, B.-H., Kim, S.-K., and Kim, S.-Y. (2019). GENT2: an updated gene expression database for normal and tumor tissues. BMC Med. Genomics *12*, 101. https://doi.org/10.1186/s12920-019-0514-7.

47. Wang, Z., Zhang, J., Zhang, Y., Deng, Q., and Liang, H. (2018). Expression and mutations of BRCA in breast cancer and ovarian cancer: Evidence from bioinformatics analyses. Int. J. Mol. Med. *42*, 3542–3550. https://doi.org/10.3892/ijmm.2018.3870.

48. Li, L., Li, S., Zhang, X., Mei, L., Fu, X., Dai, M., and Wei, N. (2024). Establishing the role of BRCA1 in the diagnosis, prognosis and immune infiltrates of breast invasive cancer by bioinformatics analysis and experimental validation. Aging *16*, 1077–1095. https://doi.org/10.18632/aging.205366.

49. Wang, G.-H., Zhao, C.-M., Huang, Y., Wang, W., Zhang, S., and Wang, X. (2018). BRCA1 and BRCA2 expression patterns and prognostic significance in digestive system cancers. Hum. Pathol. *71*, 135–144. https://doi.org/10.1016/j.humpath.2017.10.032.

50. Tsibulak, I., Wieser, V., Degasper, C., Shivalingaiah, G., Wenzel, S., Sprung, S., Lax, S.F., Marth, C., Fiegl, H., and Zeimet, A.G. (2018). BRCA1 and BRCA2 mRNA-expression prove to be of clinical impact in ovarian cancer. Br. J. Cancer *119*, 683–692. https://doi.org/10.1038/s41416-018-0217-4.

51. Guo, F., Li, C., Liu, S., Li, Z., Zhai, J., Wang, Z., and Xu, B. (2023). High BRCA1 expression is an independent prognostic biomarker in LUAD and correlates with immune infiltration. Cancer Innov. *2*, 91–95. https://doi.org/10.1002/cai2.65.

52. Mansoor, A., Kamran, H., Rizwan, H., Akhter, A., Roshan, T.M., Shabani-Rad, M.T., Bavi, P., and Stewart, D. (2024). Expression of "DNA damage response" pathway genes in diffuse large B-cell lymphoma: The potential for exploiting synthetic lethality. Hematol. Oncol. *42*, e3225. https://doi.org/10.1002/hon.3225.

53. Yan, B., Xie, B., Huang, M., Guo, J., Sun, J., Chen, J., Tao, Y., and Xiao, D. (2023). Mutations and expressions of breast cancer 1/2 in lung cancer. Thorac. Cancer *14*, 1753–1763. https://doi.org/10.1111/1759-7714.14920.

54. Wang, F., Zuroske, T., and Watts, J.K. (2020). RNA therapeutics on the rise. Nat. Rev. Drug Discov. *19*, 441–442. https://doi.org/10.1038/d41573-020-00078-0.

55. Zhu, Y., Zhu, L., Wang, X., and Jin, H. (2022). RNA-based therapeutics: an overview and prospectus. Cell Death Dis. *13*, 644. https://doi.org/10.1038/s41419-022-05075-2.

56. Quinlan, A.R., and Hall, I.M. (2010). BEDTools: A flexible suite of utilities for comparing genomic features. Bioinformatics *26*, 841–842. https://doi.org/10.1093/bioinformatics/btq033.

57. Mann, M., Wright, P.R., and Backofen, R. (2017). IntaRNA 2.0: Enhanced and customizable prediction of RNA-RNA interactions. Nucleic Acids Res. *45*, W435–W439. https://doi.org/10.1093/nar/gkx279.

58. Martin, M. (2011). Cutadapt removes adapter sequences from high-throughput sequencing reads. EMBnet J. *17*, 10. https://doi.org/10.14806/ej.17.1.200.

59. Bolger, A.M., Lohse, M., and Usadel, B. (2014). Trimmomatic: a flexible trimmer for Illumina sequence data. Bioinformatics *30*, 2114–2120. https://doi.org/10.1093/bioinformatics/btu170.

60. Langmead, B., and Salzberg, S.L. (2012). Fast gapped-read alignment with Bowtie 2. Nat. Methods *9*, 357–359. https://doi.org/10.1038/nmeth.1923.

61. Dobin, A., Davis, C.A., Schlesinger, F., Drenkow, J., Zaleski, C., Jha, S., Batut, P., Chaisson, M., and Gingeras, T.R. (2013). STAR: ultrafast universal RNA-seq aligner. Bioinformatics *29*, 15–21. https://doi.org/10.1093/bioinformatics/bts635.

62. Barnett, D.W., Garrison, E.K., Quinlan, A.R., Strömberg, M.P., and Marth, G.T. (2011). BamTools: a C++ API and toolkit for analyzing and managing BAM files. Bioinformatics *27*, 1691–1692. https://doi.org/10.1093/bioinformatics/btr174.

63. Li, H., Handsaker, B., Wysoker, A., Fennell, T., Ruan, J., Homer, N., Marth, G., Abecasis, G., and Durbin, R.; 1000 Genome Project Data Processing Subgroup (2009). The Sequence Alignment/Map format and SAMtools. Bioinformatics *25*, 2078–2079. https://doi.org/10.1093/bioinformatics/btp352.

64. Anders, S., Pyl, P.T., and Huber, W. (2015). HTSeq—a Python framework to work with high-throughput sequencing data. Bioinformatics *31*, 166–169. https://doi.org/10.1093/bioinformatics/btu638.

65. Chen, Y., Lun, A.T.L., and Smyth, G.K. (2016). From reads to genes to pathways: differential expression analysis of RNA-Seq experiments using Rsubread and the edgeR quasi-likelihood pipeline. F1000Res *5*, 1438. https://doi.org/10.12688/f1000research.8987.2.

66. Keene, J.D., Komisarow, J.M., and Friedersdorf, M.B. (2006). RIP-Chip: The isolation and identification of mRNAs, microRNAs and protein components of ribonucleoprotein complexes from cell extracts. Nat. Protoc. *1*, 302–307. https://doi.org/10.1038/nprot.2006.47.

67. Beltran, M., Tavares, M., Justin, N., Khandelwal, G., Ambrose, J., Foster, B.M., Worlock, K.B., Tvardovskiy, A., Kunzelmann, S., Herrero, J., et al. (2019). G-tract RNA removes Polycomb repressive complex 2 from genes. Nat. Struct. Mol. Biol. *26*, 899–909. https://doi.org/10.1038/s41594-019-0293-z.

68. Olive, P.L., and Banáth, J.P. (2006). The comet assay: A method to measure DNA damage in individual cells. Nat. Protoc. *1*, 23–29. https://doi.org/10.1038/nprot.2006.5.

69. Potla, P., Ali, S.A., and Kapoor, M. (2021). A bioinformatics approach to microRNA-sequencing analysis. Osteoarthr. Cartil. Open *3*, 100131. https://doi.org/10.1016/j.ocarto.2020.100131.

70. Kozomara, A., Birgaoanu, M., and Griffiths-Jones, S. (2019). miRBase: from microRNA sequences to function. Nucleic Acids Res. *47*, D155–D162. https://doi.org/10.1093/nar/gky1141.

71. Tarazona, S., Furió-Tarí, P., Turrà, D., Pietro, A.D. Di, Nueda, M.J., Ferrer, A., and Conesa, A. (2015). Data quality aware analysis of differential expression in RNA-seq with NOISeq R/Bioc package. Nucleic Acids Res. *43*, e140. https://doi.org/10.1093/nar/gkv711.

72. Yates, A.D., Achuthan, P., Akanni, W., Allen, J., Allen, J., Alvarez-Jarreta, J., Amode, M.R., Armean, I.M., Azov, A.G., Bennett, R., et al. (2020). Ensembl 2020. Nucleic Acids Res. *48*, D682–D688. https://doi.org/10.1093/nar/gkz966.

73. Smedley, D., Haider, S., Ballester, B., Holland, R., London, D., Thorisson, G., and Kasprzyk, A. (2009). BioMart – biological queries made easy. BMC Genomics *10*, 22. https://doi.org/10.1186/1471-2164-10-22.

Please cite this article in press as: Grelloni et al., BRCA1 levels and DNA-damage response are controlled by the competitive binding of *circHIPK3* or FMRP to the *BRCA1* mRNA, Molecular Cell (2024), https://doi.org/10.1016/j.molcel.2024.09.016

STAR★METHODS

KEY RESOURCES TABLE

REAGENT or RESOURCE	SOURCE	IDENTIFIER
Antibodies		
Rabbit monoclonal anti-BRCA1(A8X9F)	Cell Signaling Technology	Cat# 14823; RRID: AB_2798631
Mouse monoclonal anti-β-Actin peroxidase (clone AC-15)	Sigma-Aldrich	Cat# A3854; RRID: AB_262011
Mouse monoclonal anti-α-Actinin1 (H-2)	Santa Cruz Biotechnology	Cat# sc-17829; RRID: AB_626633
Rabbit polyclonal anti-FMRP	Abcam	Cat# ab17722; RRID: AB_2278530
Mouse monoclonal anti-FXR2	Santa Cruz Biotechnology	Cat# sc-32266; RRID:AB_627641
Rabbit monoclonal anti-PARP (46D11)	Cell Signaling Technology	Cat# 9532; RRID: AB_659884
Monoclonal anti-Flag (M2) peroxidase	Sigma-Aldrich	Cat# A8592; RRID: AB_439702
Mouse monoclonal anti-Flag (M2)	Sigma-Aldrich	Cat# F1804; RRID: AB_262044
Mouse monoclonal anti-p-Histone H2A.X (Ser 139)	Santa Cruz Biotechnology	Cat# sc-517348; RRID: AB_2783871
Anti-Rabbit IgG (H+L) Secondary Antibody, HRP	Thermo Fisher Scientific	Cat# 31460
Anti-Mouse IgG (H+L) Secondary Antibody, HRP	Thermo Fisher Scientific	Cat# 32430
Mouse monoclonal anti-HIPK2 (F-189)	Santa Cruz Biotechnology	Cat# sc-100383; RRID: AB_1124683
Rabbit polyclonal 14-3-3 epsilon (YWHAE)	Invitrogen	Cat# PA5-28937; RRID: AB_2546413
Bacterial and virus strains		
Subcloning efficiency DH5a competent cells	ThermoFisher Scientific	Cat# 18265017
Biological samples		
Tumor biopsies from primary ERMS	Department of Oncology at Alder Hey Children's NHS Foundation	09/H1002/88
Tumor biopsies from primary ARMS	Department of Oncology at Alder Hey Children's NHS Foundation	09/H1002/88
Healthy skeletal muscle biopsies	Department of Oncology at Alder Hey Children's NHS Foundation	09/H1002/88
Chemicals, peptides, and recombinant proteins		
DMEM high-glucose	Sigma-Aldrich	Cat#D6546
RPMI 1640	ThermoFisher Scientific	Cat#11875085
FBS	Sigma-Aldrich	Cat#F7524
L-glutamine	Sigma-Aldrich	Cat#G7513
Penicillin-streptomycin	Sigma-Aldrich	Cat#P0781
EGF	Corning	Cat# 354052
FGFb	Millipore	Cat# 01-106
Insulin	Sigma-Aldrich	Cat# 11376497001
MEM Non-essentials Amino Acid Solution	Sigma-Aldrich	Cat# M7145
PBS	Sigma-Aldrich	N/A
Opti-MEM Reduced Serum Medium	ThermoFisher Scientific	Cat# 31985070
Lipofectamine RNAiMAX	ThermoFisher Scientific	Cat# 13778150
Lipofectamine 2000	ThermoFisher Scientific	Cat#11668019
cOmplete, EDTA-free PIC	Roche-Merck	Cat#11873580001
DNase	ThermoFischer Scientific	Cat# EN0525

(*Continued on next page*)

Continued

REAGENT or RESOURCE	SOURCE	IDENTIFIER
1.4-Dithiothreitol (DTT)	Roche-Merck	Cat# 10708984001
4xLaemmli sample buffer	Biorad	Cat# 1610747
NuPage 4-12% Bis-Tris-Gel	ThermoFisher Scientific	Cat# NP0321BOX
NuPage 3-8% Tris-Acetate Gel	ThermoFisher Scientific	Cat# EA0378BOX
MOPS SDS Running Buffer	ThermoFisher Scientific	Cat# NP0001
Tris-Acetate SDS Running Buffer	ThermoFisher Scientific	Cat# LA0041
WesternBright ECL Chemiluminescent HRP Substrate	Advansta	Cat# K-12045
WesternBright Sirius Chemiluminescent HRP Substrate	Advansta	Cat# K-12043
PrimeScript RT Reagent Kit	TakaraBio	Cat# RR037B
SuperScript VILO cDNA Synthesis Kit Scientific	ThermoFisher	Cat#11754050
PowerUp SYBR Green Master Mix	ThermoFisher Scientific	Cat# A25742
CloneAmp HiFi PCR Premix	Clontech	Cat# 639298
Mytaq DNA polymerase	Bioline	Cat# BIO-21105
4'-Aminomethyl-4,5', 8-trimethylpsoralen hydrochloride	Sigma-Aldrich	Cat#A4330
Proteinase K	Ambion	Cat# AM2548
RiboLock RNase Inhibitor	ThermoFisher Scientific	Cat# EO0384
Streptavidin MagneSphere paramagnetic particles	Promega	Cat# Z5481
Dynabeads protein G	ThermoFisher Scientific	Cat#10003D
Trypan blue solution	ThermoFisher Scientific	Cat#15250061
α-Amanitin (A2263)	Sigma-Aldrich	Cat# 23109-05-9
Cisplatin	MedChemExpress	Cat# HY-17394
Doxorubicin	MedChemExpress	Cat# HY-15142A
Talazoparib (BMN 673)	Selleckchem	Cat# S7048
Trypan blue solution	ThermoFisher Scientific	Cat#15250061
UltraPure Ethidium Bromide	ThermoFisher Scientific	Cat#15585011
DAPI solution	Sigma-Aldrich	Cat# D9542
ProLong Diamond Antifade Mountant	ThermoFisher Scientific	Cat# P36961
Recombinant human FMRP protein	Abcam	Cat# ab132093
Ribonuclease R (RNase R)	Biosearch Technologies	Cat# RNR07250
Rnase T1	ThermoFisher Scientific	Cat# AM2283
Critical commercial assays		
In-Fusion HD Cloning Kit	Clontech	Cat# 639650
Direct-zol RNA Miniprep kit	Zymo Research	Cat# R2050
LightShift™ Chemiluminescent EMSA Kit	ThermoFisher Scientific	Cat# 20146
Deposited data		
circHIPK3 AMT-crosslinked pull-down total RNA-sequencing/circHIPK3 pull-down small RNA-sequencing	In this paper	GEO: GSE246226
Uncropped images and blots and FACS data	In this paper	DOI: https://doi.org/10.17632/fk8bm3rxh2.1
Total RNA-sequencing data for wild-type myoblasts and RD (ERMS) or RH4 (ARMS) cell lines	Dattilo et al.[15]	GEO: GSE207453
FMR1 PAR-CLIP total RNA-sequencing	Ascano et al.[11]	GEO: GSE39682

(*Continued on next page*)

Continued

REAGENT or RESOURCE	SOURCE	IDENTIFIER
ENCODE: characterization of human RBP	Van Nostrand et al.[23]	https://yeolab.com/encode
The Cancer Genome Atltas (TCGA) Program	National Cancer Institute (NCI) and National Human Genome Research Institute (NHGRI)	https://www.cancer.gov/ccg/research/genome-sequencing/tcga
Gene Expression Database of Normal and Tumor Tissues 2 (GENT2)	Park et al.[46]	http://gent2.appex.kr
Epigenetic Landscape of Rhabdomyosarcoma Subtypes	St. Jude Children's Research Hospital	https://pecan.stjude.cloud/proteinpaint/study/RHB2018
AACR Project GENIE, cBioPortal for Cancer Genomics	de Bruijn et al.[33]	https://genie.cbioportal.org
Experimental models: Cell lines		
Human male myoblasts (WT)	Telethon Biobank	N/A
Human RH4 cells	Cellosaurus	RRID: CVCL_5916
Human RD cells	ATCC	Cat# CCL-136; RRID: CVCL_1649
Human U2OS cells	ATCC	Cat# HTB-96 RRID: CVCL_0042
U2OS DR-GFP	Khurana et al.[35]	N/A
U2OS EJ5-GFP	Gunn and Stark[36]	N/A
Human A172 cells	ATCC	Cat# CRL-1620; RRID: CVCL_0131
Human SKOV-3 cells	ATCC	Cat# HTB-77; RRID: CVCL_0532
Human A549 cells	ATCC	Cat# CCL-185; RRID: CVCL_0023
Human MCF7 cells	ATCC	Cat# HTB-22; RRID: CVCL_0031
MCF7 (wt/wt)	In this paper	N/A
MCF7 wt/del	In this paper	N/A
Oligonucleotides		
DNA oligonucleotides for qRT-PCR/PCR experiments used in this work are listed in Table S4	This paper	N/A
Biotinylated DNA probes used in this work are listed in Table S4	This paper	N/A
LNA-modified oligonucleotides used in this work are listed in Table S4	This paper	N/A
siRNAs used in this work are listed in Table S4	This paper	N/A
Recombinant DNA		
pcDNA 3.1+ Mammalian Expression Vector	ThermoFisher Scientific	Cat# V79020
p-circHIPK3 BSJ	This paper	N/A
p-circHIPK3 BSJ-mut	This paper	N/A
p-circHIPK3 CTL	This paper	N/A
p-BRCA1 Ex23+3′-UTR	This paper	N/A
p-BRCA1 Ex23+3′UTR-Δ	This paper	N/A
BRCA1 Ex23+3′UTR-mut	This paper	N/A
psiCHECK-2 Vector	Promega Corporation	Cat# C8021
p-luc+HIPK3 ex2	This paper	N/A
p-luc+BRCA1 3-'UTR	This paper	N/A
RPL22 (Myc-DDK-tagged)-Human ribosomal protein L22	Origene	Cat# RC208910
pc-BRCA1	This paper	N/A
pCBAScel	Addgene	Cat# 26477

(*Continued on next page*)

Continued

REAGENT or RESOURCE	SOURCE	IDENTIFIER
Software and algorithms		
Image Lab	Bio-Rad	https://www.bio-rad.com/it-it/product/image-lab-software?ID=KRE6P5E8Z
IGV (Integrative Genomics Viewer)	Broad Institute and the Regents of the University of California	https://software.broadinstitute.org/software/igv/download
BEDTools version 2.21.0	Quinlan and Hall[56]	https://github.com/arq5x/bedtools2
IntaRNA version 2.4.1	Mann et al.[57]	http://rna.informatik.uni-freiburg.de/ IntaRNA/Input.jsp
ImageJ	NIH	https://imagej.nih.gov/ij/download.html
ImageJ Macro ''Comet Assay''	Robert Bagnell, Pathology & Lab Med UNC-CH	https://www.med.unc.edu/microscopy/resources/imagej-plugins-and-macros/comet-assay/
FACSDiva software version 6.1.3	Becton Dickinson, BD Biosciences, USA	https://www.bdbiosciences.com/en-ca/products/instruments/software-informatics/instrument-software/bd-facsdiva-software-v-6-1-3.643629
FlowJo software version 10.10.0	Becton Dickinson, BD Biosciences, USA	https://www.flowjo.com/solutions/flowjo
CatRAPID v2.1	Bellucci et al.[22]	http://s.tartaglialab.com/update_submission/755594/1b568d72ff
Cutadapt (v3.2)	Martin[58]	https://cutadapt.readthedocs.io/en/stable/
Trimmomatic (v0.39)	Bolger et al.[59]	http://www.usadellab.org/cms/?page=trimmomatic
Bowtie2 software (v2.4.2)	Langmead and Salzberg[60]	https://github.com/BenLangmead/bowtie2
STAR software (v2.7.7a)	Dobin et al.[61]	https://github.com/alexdobin/STAR
Picard suite (v2.24.1)	Broad Institute and the Regents of the University of California	https://broadinstitute.github.io/picard/
Bamtools (v2.5.1)	Barnett et al.[62]	https://github.com/pezmaster31/bamtools
Samtools (v1.7)	Li et al.[63]	http://www.htslib.org/
Htseq-count software (v0.13.5)	Anders et al.[64]	https://htseq.readthedocs.io/en/latest/
EdgeR R package (v3.34.1)	Chen et al.[65]	https://bioconductor.org/packages/release/bioc/html/edgeR.html

EXPERIMENTAL MODEL AND STUDY PARTICIPANT DETAILS

Cell cultures

All cell lines were grown at 37°C and 5% CO2. All cell lines were tested for mycoplasma contamination.

Wild-type human primary myoblasts (Telethon Biobank, obtained from a skeletal muscle biopsy of a 2-year old male child) were cultured in DMEM supplemented with 10% FBS, 2 mM L-glutamine, insulin 50 mg/ml, FGFb 25 ng/ml, EGF 1 ng/ml and penicillin-streptomycin 1X.

Human RD (embryonal rhabdomyosarcoma cell line derived from a 7-year old female patient), RH4 (alveolar rhabdomyosarcoma cell line derived from a 7-year old female patient), U2OS (osteosarcoma cell line derived from a 15-year old female patient), and modified U2OS DR-GFP and EJ5-GFP, A172 (glioblastoma cell line derived from a 53-year old male patient) and A549 (lung adenocarcinoma cell line derived from a 58-year old male patient) cells were cultured in DMEM high-glucose supplemented with 10% fetal bovine serum (FBS), 2 mM L-glutamine and 1% penicillin-streptomycin.

Human SKOV-3 cells (ovarian serous cystadenocarcinoma cell line derived from a 67-year old female patient) were cultured in RPMI 1640 medium supplemented with 10% fetal bovine serum (FBS), 2 mM L-glutamine and 1% penicillin-streptomycin.

Human MCF7 cells (invasive breast carcinoma cell line derived from a metastatic site of a 69 year old female patient) has been characterised as hyper triploid to hypotetraploid for BRCA1 gene copies (modal chromosome number 82). MCF7 cells were grown and maintained in Minimum Essential Medium Eagle supplemented with 10% fetal bovine serum, 1mM sodium pyruvate, 1x MEM Non-Essential Amino acids, 0.01mg/ml bovine insulin, 2mM L-Glutamine and penicillin/streptomycin.

We established a stable BRCA1 hemizygous cell line (clone 5-9) by deletion of two to three copies of the gene using the CRISPR/Cas9 technology as detailed below.

Please cite this article in press as: Grelloni et al., BRCA1 levels and DNA-damage response are controlled by the competitive binding of *circHIPK3* or FMRP to the *BRCA1* mRNA, Molecular Cell (2024), https://doi.org/10.1016/j.molcel.2024.09.016

Patient biopsies

Tumour samples from 8 primary RMS tumours, 3 ARMSs and 5 ERMSs, were obtained at diagnosis before any treatment from children admitted to the Department of Oncology at Alder Hey Children's NHS Foundation Trust, Liverpool, United Kingdom. Control RNA was extracted from normal skeletal muscle biopsies obtained from 3 children undergoing surgery for non-oncological conditions. Institutional written informed consent was obtained from the patient's parents or legal guardians. The study underwent ethical review and approval according to the local institutional guidelines (Alder Hey Children's NHS Foundation Trust Ethics Committee, approval number 09/H1002/88).

METHOD DETAILS

Plasmid construction

The plasmids used for the *in vitro* transcription were obtained starting from the pcDNA 3.1 (+) Mammalian Expression Vector (ThermoFisher Scientific, Cat#V79020). BRCA1 exon 23+3′-UTR (nucleotides 5581-5880of BRCA1 mRNA), circHIPK3 BSJ region (nucleotides 1000-99) and circHIPK3 CTL region (nucleotides 454-658) were PCR-amplified from RD cDNA, using respectively BRCA1 exon 23+3′-UTR Fw&Rv, circHIPK3 BSJ Fw&Rv and circHIPK3 CTL Fw&Rv oligonucleotides. The pcDNA vector was opened by inverse PCR using pcDNA 3.1 (+) INV Fw&Rv oligonucleotides. The DNA fragments were then cloned into the pcDNA vector downstream of the T7 promoter using the In-Fusion HD Cloning Kit (Clontech), obtaining the p-BRCA1 Ex23+3′-UTR, p-circHIPK3 BSJ and p-circHIPK3 CTL plasmids.

To generate p-BRCA1 Ex23+3′UTR-Δ (nucleotides 5581-5595/5634-5880), the sequence interacting with circHIPK3 BSJ in BRCA1 Exon 23 (5596-5633), was removed by inverse PCR using 5′-phosphorylated BRCA1 Ex23+3′-UTR Δ_circ Fw & Rv oligonucleotides, and then the final plasmid was obtained by self-ligation of the PCR product.

To generate BRCA1 Ex23+3′UTR-mut plasmid, inverse PCR of p-BRCA1 Ex23+3′UTR was performed to linearize the plasmid and to remove circHIPK3 interaction site present in BRCA1 Ex23+3′ UTR (nucleotides 5596-5633), using 5′-phosphorylated BRCA1 Ex23+3′-UTR-mut Fw&Rv oligonucleotides. After subsequent self-ligation, a random sequence of 37 nucleotides (added to BRCA1 Ex23+3′-UTR-mut Fw&Rv oligonucleotides) was inserted in the place of circHIPK3 interaction site. In the same way, a sequence complementary to this mutation has been inserted in p-circHIPK3 BSJ, after the removal of the BRCA1 interacting site (nucleotides 1068-1099 and 1-13) through inverse PCR using 5′-phosphorylated circHIPK3 BSJ-mut Fw&Rv oligonucleotides, generating p-circHIPK3 BSJ-mut.

P-luc+HIPK3 Ex2 and p-luc+BRCA1 3′-UTR constructs were obtained starting from the psiCHECK-2 vector (Promega Corporation; Cat# C8021), and we referred to it as p-luc. HIPK3 exon 2 was PCR-amplified from RD cDNA using HIPK3 ex2 Fw&Rv oligonucleotides, while BRCA1 3′-UTR (nucleotides 5706-7088) was PCR-amplified from RH4 genomic DNA with BRCA1 3′-UTR Fw&Rv oligonucleotides. The psiCHECK-2 vector was opened by inverse PCR using psiCHECK-2 INV Fw&Rv oligonucleotides. The DNA fragments were then cloned into the psiCHECK-2 vector downstream of the Renilla luciferase using the In-Fusion HD Cloning Kit (Clontech).

To generate the vector used for the ectopic expression of BRCA1, BRCA1 CDS was inserted in pcDNA 3.1 (+) plasmid in two steps. Firstly, RD RNA was retrotranscribed in cDNA using oligonucleotides specific for BRCA1 CDS (BRCA1 CDS1 Fw and BRCA1 CDS2 Rv). Then, nucleotides 1-2805 and 2806-5589 of BRCA1 CDS were PCR amplified from the previously mentioned cDNA, using respectively oligonucleotides BRCA1 CDS1 Fw&Rv and BRCA1 CDS2 Fw&Rv. The pcDNA 3.1 (+) vector was opened by inverse PCR using pcDNA 3.1 (+) INV Fw&Rv oligonucleotides. The first fragment of BRCA1 CDS was cloned into pcDNA 3.1 (+) by In-Fusion HD Cloning Kit (Clontech). Following that, the plasmid obtained was linearized by inverse PCR using BRCA1 CDS1 INV Fw and pcDNA 3.1 (+) INV Rv oligonucleotides. Finally, the second fragment of BRCA1 CDS was cloned by In-Fusion HD Cloning Kit (Clontech), obtaining the p-BRCA1 plasmid.

CloneAmp HiFi PCR Premix (Clontech) was used to perform all the PCR reactions needed to obtain these plasmids, according to the manufacturer's instructions. The oligonucleotides used are listed in Table S4.

Rnase R treatment

RNase R treatment was performed as follows: 1 μg of total RNA was diluted in 20 μL of water with 1u RNase R/μg and 2 μL of enzyme buffer (LGC Biosearch Technologies), then incubated 10 min at 37°C and purified by phenol-chloroform extraction.

Cell transfection

30 nM of siRNA (ON-TARGETplus, Dharmacon), 200 nM of miRNA-blockers LNA, 5 nM (for RD cells) or 20 nM (for MCF7 cells) of LNA (Integrated DNA Technologies) were transfected with Opti-MEM and Lipofectamine RNAiMAX Transfection Reagent (Invitrogen), according to the manufacturer's instructions. Unless differentially specified, the medium was replaced 6 h after transfection and cells were harvested 48 h after transfection. siRNAs and LNAs used in this work are listed in Table S4.

For CRISPR/Cas9, MCF7 cells were transfected by electroporation using the Lonza Nucleofector™ Transfection 2b Device.

sgRNAs, ssODN, and primers

Synthetic single guide RNAs (sgRNAs) targeting sites at either the 5′ or 3′ untranslated regions (UTRs) of BRCA1 gene (sgRNA-5′UTR (#5791) sgRNA-3′UTR (#5801)) were designed using the CRISPick online utility (https://portals.broadinstitute.org/gppx/crispick/public)

and obtained from Synthego Sequences. sgRNAs sequences are listed in Table S4. An 86bp-long single-stranded antisense oligodeoxynucleotide repair template (ssODNA #5814) with homology arms to either side of the targeted loci was designed to paste together the two non-adjacent DNA ends. A *BamHI* site was also introduced in the ssODNA sequence to facilitate the identification of alleles repaired by homology-directed repair (HDR). The sequence of ssODNA and oligos designed for the identification of BRCA1 hemizygous cell clones are detailed in Table S4

CRISPR/Cas9-mediated generation of BRCA1 hemizygous MCF7 cells

To delete a 80.2 kb genomic fragment encompassing the entire BRCA1 gene body, MCF7 cells were nucleofected with two CRISPR/Cas9 RNA-guided ribonucleoprotein (RNP) complexes targeting the 5′ and 3′ UTR regions, along with the bridging ssODN #5814. RNP complexes were preformed by mixing Cas9 protein (20μg) with the sgRNAs #5791 and #5801 (250 pmoles each) in 20μL of nucleofection buffer and incubated for 10-20 min at room temperature. Subsequently, two million cells were nucleofected in a total volume of 100μL of nucleofection buffer containing the two RNP complexes plus 400 pmoles of the bridging ssODN #5814 using the program P-020. Cells were allowed to recover and expanded for 10 days before subcloning at limiting dilution in 96-well plates. Clones with at least one deleted copy of the BRCA1 gene were selected by PCR using primers #5815-Fwd and #5816-Rev.

To determine the BRCA1 copy number, genomic DNAs from selected clones were analysed by ddPCR using the QX100™ Droplet Digital PCR System platform. Specifically, ddPCR Copy Number validated assay for BRCA1 (Biorad: dHsaCP2500367) was used. BRCA1 was detected with FAM probes and reference gene RPP30 with HEX. PCR reactions were performed using 10 ng of gDNA and ddPCR Supermix for Probes according to the manufacturer's instructions. Droplets were generated by loading reaction mixtures and Droplet Generation Oil for Probes into a DG8 Cartridge using a QX200 Droplet Generator (BioRad Laboratories, Hercules, CA, USA). Samples were carefully transferred in-plate, sealed, and run on a C1000 Thermocycler (Biorad). Finally, the plates were transferred in the QX200 Droplet Reader and data were acquired and analysed using QuantaSoft software (Biorad).

Western blot

Cells were detached with Trypsin-EDTA 1X and centrifuged at 1500 rpm for 5 minutes. Pellets were resuspended in Protein Extraction Buffer (100 mM Tris pH 7.5, EDTA 1 mM, SDS 2%) supplemented with PIC 2X (Complete- EDTA free, Roche–Merck), incubated 30 min at 4°C on a rotating wheel and centrifuged at 15000g for 15 min at 4°C. Proteins (20-30 μg for most of the experiments, quantified through Bradford reagent (Bio-Rad Protein Assay)) were heated 5′ at 80°C for denaturation, incubated 5′ in ice and were loaded on 4%-12% bis-tris-acrylamide gel or, in case of BRCA1 detection, 3-8% Tris-acetate gel (ThermoFisher Scientific) for a 1-1.5h running process at 150V.

Proteins were transferred to a nitrocellulose membrane through a 1-2h blotting process at 400 mA with BioRad blotting apparatus and a 20% methanol buffer. The membrane was blocked in 5% milk and hybridized with the specific primary antibody overnight at 4°C or 1 h at room temperature for HRP antibodies. Membranes hybridized with non-HRP antibodies, were then hybridized the morning after with the appropriate secondary antibody (Invitrogen) for 1-2 h at room temperature. Protein detection was carried out with WesternBright® ECL Chemiluminescent HRP Substrate (Advansta) or with WesternBright® Sirius Chemiluminescent HRP Substrate (Advansta). Images were acquired with ChemiDoc MP Imager (Bio-Rad) and the analysis was performed using Image Lab 5.2.1 software (Bio-Rad). Images were linearly adjusted in contrast and brightness when necessary. Antibodies are listed in key resources table. Uncropped images are available in supplemental information.

RNA isolation and analysis

For most of the experiments, total RNA was extracted with Direct-zol RNA Miniprep kit (Zymo Research) with a 15-minute DNase-I treatment according to the manufacturer's protocol. For IP and RNA pull-down experiments, and polysome fractionation experiments, RNA was precipitated through phenol/chloroform extraction.

RNA was subjected to reverse transcription with PrimeScript RT Reagent Kit (Takara Bio), or, in case of RNA pull-down and IP experiments, with SuperScript VILO cDNA Synthesis Kit (ThermoFisher Scientific), both used according to the manufacturer's protocol.

For qRT-PCR, PowerUp SYBR Green Master Mix reagent (ThermoFisher Scientific) was used according to the manufacturer's instructions. RNA levels are relative to GAPDH mRNA unless differently specified. Relative RNA quantity was calculated as the fold change ($2^{\wedge}$-ΔΔCt) with respect to the control sample set as 1, unless differently specified.

The efficiency of qRT-PCR primers was calculated based on a standard curve made from serial dilutions of RD cDNA, followed by qPCR with a specific pair of oligonucleotides. Then, the slope of the standard curve was used to calculate the amplification efficiency of each qPCR reaction. Here are reported the efficiencies of the most used qRT-PCR primers: circHIPK3 (E=109.03%), linHIPK3 (E=95.18%), BRCA1 (E=100.86%) and GAPDH (E=102.84%). Oligonucleotides used for qRT-PCR are listed in Table S4.

RNA pull down

For native RNA-pull-down protocol, 10-15x10^6 cells for each biological replicate were pelleted and resuspended in 1 ml of cold Lysis Buffer (Tris-HCl pH 7.5 50mM, NaCl 150mM, $MgCl_2$ 3mM, NP40 0.5%, EDTA 2mM) supplemented with PIC 1X, RNAse Inhibitor 1:400, DTT 1mM. Cells were passed through a 27 gauge needle 4 times and incubated 30' at 4°C on a rotating wheel to allow nuclear lysis. Lysate was centrifuged 15' at 4°C at 1500g. The same volume of supernatant was taken for target (circHIPK3 or HIPK3) and LacZ (negative control) pull downs and 10% of pull-down volume was saved as input condition. For every pull-down reaction, a

double volume of cold Hybridization Buffer (Tris-HCl pH 7.5 1000mM, NaCl 300mM, $MgCl_2$ 1mM, NP40 0.5%, EDTA 10mM, SDS 0.2%, Formamide 15%) supplemented with PIC 1X, RNAse Inhibitor 1:400, DTT 1mM was added. 200 pmol of biotinylated probes mix dissolved in 50 μl of Lysis Buffer, heated at 80°C for 3′ and then transferred in ice, were added in each pull-down reaction and samples were incubated 4h at 4°C on a rotating wheel. Therefore, 100 μl of pre-washed streptavidin beads (Promega) were added and samples were incubated 2h at 4°C on a rotating wheel.

For RNA pul ldown in si-scr or si-circHIPK3 condition, $2x10^6$ RD cells were plated in two 10-cm plates, transfected the morning after with 30 nM of si-SCR and si-circHIPK3 respectively, moved to 15-cm plates 24h post-transfection and pelleted for the pull down 48h after transfection.

For AMT-crosslinked RNA-pull-down protocol, $40x10^6$ RD cells for each biological replicate were pelleted, resuspended in 1 ml of cold PBS supplemented with 0.5 mg/ml of 4'- aminomethyl-4,5',8-trimethylpsoralen (AMT, Cayman Chemical) per $1x10^7$ cells and crosslinked at 365 nm for five 2-minute cycles. 1 volume of Guanidinium Hydrochloride 6M per each volume of AMT was added. The lysate was subdivided into 250μl aliquots. 12,5 μl of a 20 mg/mL solution of Proteinase K (Ambion), 6.5 μL of 20% SDS and RNAse Inhibitor 1:250 were added to each aliquot and the samples were incubated at 65°C for 1 h. RNA was precipitated through phenol/chloroform extraction, subjected to DNAse I treatment and re-extracted. RNA extracted post DNAse treatment was equally divided in three tubes, one per pull down (LacZ, ODD, EVEN) and 10% of every fraction of RNA was taken and considered as input, while the rest was brought to a volume of 500 μL with RNAse free water, incubated 2' at 98°C and put in ice. For every pull down, 500 pmoles of biotinylated probes (4 ODD probes, 4 EVEN probes, 4 LacZ probes, listed in Table S4), 500 μL of 2X binding buffer (Tris-HCl 20mM, NaCl 1M, EDTA 2mM, SDS 0.1%) and 4μL of RNAse Inhibitor were added to RNA. The mixes were heated at 65°C for 3′ and then incubated 4h on a rotating wheel at room temperature. Then, 500 μL of Streptavidin beads (Promega), resuspended in 1X binding buffer, and 2μL of RNAse Inhibitor, were added and RNA-probes-beads mixes were incubated 2h on a rotating wheel at 4°C. Finally, beads were washed two times with 1X binding buffer and two times with 1X wash buffer (Tris-HCl 10mM, NaCl 200mM, EDTA 1mM, SDS 0.05%) and 1 mL of TRIzol was added for each sample.

RNA immunoprecipitation

The RNA-immunoprecipitation (RIP) assays for FMRP, FXR2 and RPL22-FLAG protein were performed in RD cells following the protocol described in Keene et al.[66]

For RPL22-FLAG immunoprecipitation in si-scr or si-circHIPK3 condition, $2x10^6$ RD cells were plated in two 10-cm plates and transfected the morning after with 10 μg of RPL22 (Myc-DDK-tagged)-Human ribosomal protein L22 plasmid plasmid (Origene, Cat# RC208910). 6 h after transfection, RPL22-FLAG-transfected cells were split into two 10-cm plates and the following morning were transfected with either 30 nM si-scr or 30 nM si-circHIPK3. 48 h after siRNA transfection, cells were harvested and the RIP assay with Dynabeads Protein G was performed. 20% of each lysate was saved as input. Half of the remaining lysate was used to precipitate RPL22-FLAG with 2 μg of FLAG antibody, while for the other half 2 μg of IgG antibody was used as a negative control. 15% of what was immunoprecipitated with each antibody was used to analyze the levels of the flagged protein precipitated, while the remaining 75% was used to examine the RNAs associated to the ribosomal flagged protein.

Cross-linking immunoprecipitation(CLIP) was performed according to Beltran et al.[67] with the following modifications. A total of $2.5x10^7$ RD cells per UV RNA immunoprecipitation (CLIP) were irradiated with 0.4 J/cm2 of 254 nm UV light. Cells were lysed and treated for fragmentation with Turbo DNase (4 μL) and RNAse T1 (10 μL of a dilution 1/500) for 3 minutes at 37 degrees. Lysate was cleared by centrifugation and 5 μg of antibody coupled to Dynabeads Protein G were added. After 4h incubation beads washed 3 times with wash buffer containing 1000 mM NaCl, pelleted and then incubated in 200 mL PK buffer (100 mM Tris-HCl pH 7.4, 50 mM NaCl and 40 mL Proteinase K) for 20 min at 1100 rpm and 37°C. An equal volume of PK buffer containing 7 M urea was added, and a second incubation was performed. Supernatant was collected, and RNA was purified via phenol-chloroform extraction. 10% of each lysate was saved prior proteinaseK treatment to check protein enrichment by western blot. Oligonucleotides used for qRT-PCR are listed in Table S4.

Antibodies used for RNA-immunoprecipitation are listed in key resources table.

Drug treatment

For Cisplatin (MedChemExpress), Doxorubicin (MedChemExpress) or Talazoparib (SelleckChem) treatment,$1x10^5$ -$1,5x10^5$ cells for well were seeded in 12 well plates. Cells were transfected with siRNAs or LNAs the day after, treated with the drug 24h from transfection and, finally, detached with Trypsin-EDTA 1X and counted 24, 30 or 48h after the treatment with Trypan blue to consider only the living ones. The percentage of survival was calculated by dividing the number of living treated cells with the number of living non-treated cells, transfected with the same siRNA, multiplied by 100. For Cisplatin and Doxorubicin experiments, cells were pelleted after the count and resuspended in Protein Extraction Buffer (100 mM Tris pH 7.5, EDTA 1 mM, SDS 2%) supplemented with PIC 2X (Complete- EDTA free, Roche–Merck) for protein extraction.

For alpha-amanitin treatment (Sigma-Aldrich), $5x10^5$ cells were seeded in each of two 6 cm-plate. Cells of each 6 cm-plate were transfected with siRNAs the day after, split in 3 well (0h,5h,10h) of a 12-well plate 24h from transfection and treated with alpha-amanitin 25 μg/ml (in fresh medium) 48h after transfection. 0h cells were harvested with TRIzol before treatment, while 5h and 10h cells were harvested respectively 5 and 10h after treatment. Graphs represent fold changes calculated as 2-DCt, normalized to the reference sample (0 h) which was set as 1.

Polysome fractionation

Sucrose gradients were prepared the day before cells harvesting by carefully adding in a tube decreasing concentrations of sucrose (50% to 10%) and kept at 4°C over-night.

48h post si-RNAs transfection, 10-15x10^6 cells for each condition were treated for 15' with 100 μg/ml Cycloheximide, pelleted and resuspended in 430 μl of Polysome Extraction Buffer (Tris-HCl 20mM, KCl 100mM, MgCl2 5mM, NP40 0.5%) supplemented with PIC 1X, RNAse Inhibitor 1:200, 100 μg/ml Cycloheximide. Lysates were kept 10' in ice, centrifuged 10' at 4°C at 12000g and supernatants (cytoplasmatic fractions) were carefully added on the top of sucrose gradients. Tubes were ultra-centrifuged for 2h at 4°C at 37000 rpm. After ultra-centrifugation, each sample was divided in 100 μl fractions and the 260nm absorbance was measured. Absorbance vs density graph was plotted and fractions were separated according the profile. A spike RNA was added in each fraction. The amount of RNA, detected for qRT-PCR, for each fraction was normalized to spike levels and considered as a percentage of the total amount of RNA, obtained by summing the quantity of RNA present in each fraction.

Immunofluorescence

8x10^4 RD cells cultured on pre-coated glass coverslips (0.4 mg/ml Collagen Rat Tail, Corning) were transfected the morning after with 30 nM si-scr or 30 nM si-circHIPK3. 48h post transfection, cells were fixed in 4% paraformaldehyde in warm PBS for 15 min at room temperature, washed three times with warm PBS and then blocked and permeabilized for 60 min at room temperature with a blocking buffer (PBS with 5% BSA, 0.3% Triton X-100).

Cells were hybridized overnight with anti-γ H2AX Ser139 primary antibody (Santa Cruz Biotechnology) diluted 1:200 in a dilution buffer (PBS with 1% BSA, 0.3% Triton X-100). The morning after, behind five washes in PBS, cells were hybridized with fluorescent goat anti-mouse IgG (H+L) cross-adsorbed secondary antibody (Alexa Fluor 488; ThermoFisher Scientific) and DAPI solution (Sigma-Aldrich), diluted respectively 1:200 and 1:5000 in the same dilution buffer, for 2 h. Cells were, then, washed again three times with PBS and coverslips were mounted on microscope slides using ProLong Diamond Antifade Mountant (ThermoFischer Scientific). Images were acquired with Zeiss Axio Observer A1 Inverted Microscope and processed only in intensity threshold, contrast, and brightness on ImageJ software.

Flow cytometry

For NHEJ and HR repair reporter assays, 2x10^5 U2OS EJ5-GFP or U2OS DR-GFP cells were seeded in 6 well plates and transfected with siRNAs (si-scr, si-circHIPK3, si-BRCA1) the day after. 24h post RNA interference, for each siRNA, half of the cells was not transfected, while the other half was transfected with 1μg of plasmid expressing I-SceI nuclease. Cells were harvested 72h after siRNA transfection and resuspended into single cell suspension for flow cytometry experiments performed using Becton Dickinson (BD) instrument LSRFortessa (Becton Dickinson, BD Biosciences, USA) equipped among others with a 488nm Solid Sapphire 488/50 laser (Becton Dickinson, BD Biosciences, USA). Samples were acquired using FACSDiva software (BD Biosciences, version 6.1.3) and analyzed using FlowJo software (BD Biosciences, version 10.10.0).

A total of 50,000 events/sample were collected.

In vitro transcription and electrophoresis mobility shift assay

For *in vitro* transcription, pCDNA 3.1 vectors containing the region of interest downstream of T7 promoter were digested 1h with *NotI* for linearization and gel purified. 1μg of linearized transcript was used for in vitro transcription using MEGAscript T7 kit (ThermoFisher Cat#AM1334). For biotin-labeled transcripts biotin-16-UTP (ThermoFisher cat#AM8452) was added to the reaction. Reaction was performed 4h at 37°, followed by DNase treatment and phenol-chloroform purification, correct size and possible degradation was checked by running samples in a TBE 5% Acrylamide gel 7M Urea.

LightShift Chemiluminescent RNA EMSA kit (ThermoScientific cat#20158) was used to perform mobility shift assay. Briefly 5nM of biotinylated oligos, or 0,5-2,5, 25 nM of competing transcripts were mixed in Binding Buffer (10mM HEPES 7.3, 20mM KCl, 1mM MgCl2, 1mM DTT, 1mg/mL tRNA and RNAseOUT). Samples were incubated 2' at 80° and 2' on ice ensure denaturation, and binding rection was performed for 30 minutes at room temperature. For competition assays with FMRP1 protein, 5nM of biotinylated oligos and 25nM of competing transcripts were incubated as previously described. After denaturation 50nM of recombinant human FMRP protein (Abcam ab132093) was added to the reaction and incubation was carried out for 30 minutes at 4°. Non-denaturing RNA loading buffer was added to the reaction and samples were loaded in a 5% TBE gel Acrylamide gel and run in 4° 0.5X TBE for 2 hours at 100V. Electro transfer against a nylon membrane was carried out using cold 0.5X TBE at 400mA for 30 minutes, and samples were crosslinked using 480mJ/cm2 254nm UV light. Images were acquired with ChemiDoc MP Imager (Bio-Rad) as previously described. For control loading images, a part of the reaction was saved and denatured with formamide-containing loading buffer, heated 80° 2 minutes and loaded Ethidium bromide agarose gel for imaging.

Absolute copy number quantification

CircHIPK3 and *BRCA1* mRNA copy number per cell was calculated based on a standard curve made from serial dilutions of retro-transcribed RNA fragments "circHIPK3 BSJ" and "BRCA1 ex23+3′UTR" starting from 9x10^9 circHIPK3 and 6.25x10^9 BRCA1 molecules per reaction with the following oligos;

Hipk3 Fw; circHIPK3 BSJ Rv; BRCA1 ex23+3′-UTR and BRCA1 quantRv. Sequences are listed in Table S4.

$4x10^5$ RD cells were harvested in Trizol reagent and RNA isolated according to manufacturer's protocol. Amount of RNA per cell was calculated based on the extraction results. RNA was subjected to reverse transcription with PrimeScript RT Reagent Kit (TakaraBio). qRT-PCR was performed with 50ng of cDNA, using PowerUp SYBR Green Master Mix reagent (ThermoFisher Scientific) and beforementioned oligonucleotides.

COMET assay

COMET assay was performed as described in Olive and Banáth protocol.[68] Cells were dissolved in low temperature melting agarose and loaded on a frosted-end microscope slide. Cell lysis was performed in alkaline conditions (1.2 M NaCl, 100 mM Na2EDTA, 0.1% sodium lauryl sarcosine, 0.26 M NaOH) and electrophoresis was run in 0.03 M NaOH, 2 mM Na2EDTA solution. Nuclei were stained for 20 minutes at room temperature using Ethidium Bromide solution; then slides were rinsed with distilled water to remove excess stain. Slides were imaged on a Zeiss AXIO Observer A1 microscope. Comet tail moment was measured using the ImageJ Macro "Comet Assay". RD cells were transfected with si-scr or si-circHIPK3 siRNAs; after 6 h, they were transfected with either 4000 ng of empty pcDNA 3.1 (+) plasmid or p-BRCA1. Four independent biological replicates of this experiment were performed at 48 h after siRNAs transfection. Otherwise, MCF7 wt/wt and wt/del cells were transfected with LNA scr or LNAex23. The experiment was performed at 48 h after transfection as well, in four independent biological replicates.

Luciferase assay

$4x10^4$ RD cells were seeded in 24-well plates and cultured until 70% confluency. Afterwards, cells were transfected with si-SCR, si-circHIPK3 or si-linHIPK3. 6 hours after siRNA transfection, cells were transfected with 20 ng of p-luc, p-luc+HIPK3 Ex2 or p-luc+BRCA1 3′-UTR using Lipofectamine™ 2000 Transfection Reagent (ThermoFisher Scientific, Cat#11668019). After 48 hours, cells were washed twice with 250 μL of fresh PBS, 125 μL of Passive Lysis Buffer (Promega, Cat# E1910) was added and lysis was allowed to occur in oscillation at 4°C for 15 minutes. Then cells were spun to precipitate biological membranes and 10 μL of sample were plated in a 96-multiwell. Finally, firefly luciferase activity was measured using a dual-luciferase reporter assay system (Promega, Cat# E1910) and normalized to the Renilla value.

circHIPK3 pull-down microRNA-seq analysis

QIAseq miRNA library kit (QIAGEN, Hilden, Germany) has been used for library preparation following the manufacturer's instructions. RNA samples were quantified, and quality tested by Agilent 2100 Bioanalyzer RNA assay (Agilent technologies, Santa Clara, CA) or Caliper (PerkinElmer, Waltham, MA). Final libraries were checked with both Qubit 2.0 Fluorometer (Invitrogen, Carlsbad, CA) and Agilent Bioanalyzer DNA assay or Caliper (PerkinElmer, Waltham, MA). Libraries were then prepared for sequencing and sequenced on single-end 150 bp mode on NovaSeq 6000 (Illumina, San Diego, CA). RNA-seq fastq processing and microRNAs quantification from were performed according to Potla et al.[69] using miRbase (v22) reference sequences.[70] Differential abundance analysis was performed comparing EVEN, ODD or LACZ pull-down samples to INP sample through edgeR R package (v3.34.1)[65] using exact test (indicated pipeline without replicates) and NOISeq software (v2.36.0).[71] Circ HIPK3 bound miRNAs were identified as those significantly enriched in the pull-down (EVEN or ODD) VS Input contrast, but not in the lacZ VS Input comparison. Enriched miRNAs were defined as those with $\log_2$ fold-enrichment > 1.5 (pull down vs Input) and FDR < 0.05 in edgeR analysis and probability > 0.95 in NOISeq analysis. In order to obtain more stringent results, $\log_2$ fold-enrichment threshold in the lacZ VS Input comparison was set at > 0.

circHIPK3 pull-down RNA-seq analysis

Duplicated replicates of circ-HIPK3 pull-down experiment were prepared together with duplicated Input samples (INP). For pull-down samples three distinct sets of probes were used: Even (EVEN), Odd (ODD) and lacZ control (LACZ).

RNA library was produced using Stranded Total RNA Prep with Ribo-Zero Plus (Illumina). All samples were sequenced on an Illumina Novaseq 6000 Sequencing system.

Cutadapt (v3.2)[58] with parameters: -u 1 -U 1 –nextseq-trim=20 –trim-n and Trimmomatic (v0.39)[59] with parameters: -PE ILLUMINACLIP:adapter_path:2:30:10:8:3:true LEADING:3 TRAILING:3 SLIDINGWINDOW:4:20 were used to remove adapter sequences and poor quality bases; for both software the minimum read length after trimming was set to 35. Reads aligning to rRNAs were filtered out; this first alignment was performed using Bowtie2 software (v2.4.2).[60] Then, STAR software (v2.7.7a)[61] was used to align reads to GRCh38 genome using the following parameters: –outSAMstrandField intronMotif –outSAMattrIHstart 0 –outFilterType BySJout –outFilterMultimapNmax 20 –alignSJoverhangMin 8 –alignSJDBoverhangMin 1 –outFilterMismatchNmax 999 –outFilterMismatchNoverLmax 0.04 –alignIntronMin 20 –alignIntronMax 1000000 –alignMatesGapMax 1000000 –outFilterIntronMotifs RemoveNoncanonical –peOverlapNbasesMin 50. PCR duplicates were removed from all samples using MarkDuplicates command from Picard suite (v2.24.1) (https://broadinstitute.github.io/picard/) and multi-mapped and un-properly paired reads were filtered out using bamtools (v2.5.1)[62] and samtools (v1.7)[63] respectively. Gene quantification of RNA fragments was performed using htseq-count software (v0.13.5)[64] with the following parameters -s reverse -m union and using Ensembl gene annotation (release 99).[72]

Differential abundance analysis was performed comparing circ-HIPK3 pull down (EVEN, ODD) or control lacZ pull down (LACZ) to Input (INP) through edgeR R package (v3.34.1) 3. Genes with less than 10 reads in at least 2 samples for each comparison (EVEN vs INP; ODD vs INP and LACZ vs INP) were filtered out. TMM normalization was used to normalize samples between sets while model

fitting and testing was performed using the glmFIT and glmLRT functions. Genes with average FPKM < 1 in both compared sets were filtered out. Circ-HIPK3 pull down enriched transcripts were identified as those significantly enriched (log_2 fold-change > 1.5 and FDR < 0.05) in the circ-HIPK3 pull down (EVEN or ODD) vs Input (INP) contrast, but not in the lacZ vs Input comparison. in order to obtain more stringent results, log_2 fold-change enrichment threshold in the lacZ VS Input comparison was set at > 0.

RNA-RNA interaction prediction

RNA-RNA interaction prediction was performed using IntaRNA 2 software[57] with default parameters.

Interaction prediction was performed using circHIPK3 sequence as query and pull down or control RNA group as target.

In order to include the back splicing junction in RNA-RNA predictions, circHIPK3 sequence (HIPK3 exon 2) was extended by 150 nucleotides repeating the first part of the sequence. In order to avoid RNA sequence redundancy in genes with multiple isoforms, the longest functional isoforms was selected as representative for each locus. RNA sequences were retrieved from Ensembl (release 99) using Biomart software.[73] Control group was generated selecting for each pull down RNA 3 controls with the following features (Figure S3A): expressed more than 1 FPKM in the input; not enriched in pull down (with log_2 FC PD/INP < 0 in EVEN and in ODD); with the same biotypes; finally, the RNAs with the most similar length were selected. For mRNA also the control with the most similar length of functional regions was selected. The similarity between the pull-down and control length distribution was assessed using the Mann Whitney U test (*p* value > 0.05).

circHIPK3 contacts enrichment analysis (Figure S3B) was performed as follow: bins related to circHIPK3 sequence were generated using a 50 nucleotides sliding window with 1 nucleotide step and then intersected with the predicted RNA interactions using bedtools suite[56] in order to obtain for each bin the amount of RNA contacts for pull-down and control RNA groups. Then for each bin a 4x4 contingency table was compiled using the amount of interacting or not interacting RNAs in the pull-down or control group. Log_2 Odds-ratio was used to measure the contacts enrichment in pull-down over control groups while enrichment significance was assessed using Fisher's exact test.

QUANTIFICATION AND STATISTICAL ANALYSIS

The distribution and deviation of data shown in the figures of this work, the statistical tests used to calculate significant differences, and the exact value of n (e.g., the number of biological replicates of the experiments) are denoted in figure legends. When possible, individual data points from biological replicates were depicted as dots in the graphs. In main figure legends, SE stands for standard error and SD stands for standard deviation.

For Figure 1B. Data are represented as mean ±SD.Two-tailed unpaired Student's t test tested the ratio of each sample versus control.

For Figure 2. Data are represented as mean (For Figures 2B and 2C), or mean of enrichment versus input (2D and 2E) ±SD and two-tailed unpaired (for Figures 2B and 2C) Student's t test tested the ratio of each sample versus control. See also Figure S2.

For Figure 3F. Data are represented as mean of relative protein levels ±SD. Two-tailed unpaired Student's t test tested the ratio of each sample versus control.

For Figure 4: for Figures 4D and 4E, data are shown as mean of enrichment versus input ±SD. Two-tailed paired Student's t test tested the ratio of each sample versus control.

For Figure 5: Data are represented as mean of fold changes (Figures 5A–5C), or of enrichment versus input (Figures 5D and 5E) ±SD. For polysomes fractionation (Figures 5F and 5G), data are represented as percentage of RNA related to total RNA.

Two-tailed unpaired (Figures 5A–5C) or paired (Figures 5D–5G) Student's t test tested the ratio of each sample versus control.

For Figure 6: Data are represented as mean of relative protein levels in Figures 6B, F right, G right, ±SD. Two-tailed unpaired (Figures 6B, 6F right, and 6G right) or paired (Figures 6A, 6C–6F left, 6G left, and 6H) Student's t test tested the ratio of each sample versus control.

For Figure 7: Data are represented as mean of fold changes (RNA and protein quantification), or of enrichment versus input (for RNA pull down) ±SD. Two-tailed unpaired (protein and RNA quantification) or paired (drug sensitivity and COMET assay) Student's t test tested the ratio of each sample versus control

Significance values were depicted in the figures using the following key legend: *: p <0.05, **: p <0.01, ***: p <0.001. The exact *p* values of statistical confrontations shown in the main figures are indicated in the corresponding figure legend.